ARTICLES
https://doi.org/10.1038/s41556-019-0321-6
nature cell biology

The lysosomal GPCR-like protein GPR137B regulates Rag and mTORC1 localization and activity

Lin Gan[1,4], Akiko Seki[1,4], Kimberle Shen[2], Harini Iyer[2], Kyuho Han[1], Arnold Hayer[1], Roy Wollman[3], Xuecai Ge[1], Jerry R. Lin[1], Gautam Dey[1], William S. Talbot[2] and Tobias Meyer[1*]

Cell growth is controlled by a lysosomal signalling complex containing Rag small GTPases and mammalian target of rapamycin complex 1 (mTORC1) kinase. Here, we carried out a microscopy-based genome-wide human short interfering RNA screen and discovered a lysosome-localized G protein-coupled receptor (GPCR)-like protein, GPR137B, that interacts with Rag GTPases, increases Rag localization and activity, and thereby regulates mTORC1 translocation and activity. High GPR137B expression can recruit and activate mTORC1 in the absence of amino acids. Furthermore, GPR137B also regulates the dissociation of activated Rag from lysosomes, suggesting that GPR137B controls a cycle of Rag activation and dissociation from lysosomes. GPR137B-knockout cells exhibited defective autophagy and an expanded lysosome compartment, similar to Rag-knockout cells. Like zebrafish RagA mutants, GPR137B-mutant zebrafish had upregulated TFEB target gene expression and an expanded lysosome compartment in microglia. Thus, GPR137B is a GPCR-like lysosomal regulatory protein that controls dynamic Rag and mTORC1 localization and activity as well as lysosome morphology.

Cells regulate growth, autophagy and metabolism by employing a lysosomal regulatory complex consisting of heterodimers of Rag small GTPase proteins (one RagA/B protein paired with one RagC/D protein)[1–3] and the cytoplasmic regulatory complex mechanistic target of rapamycin complex 1 (mTORC1) containing the protein kinase mTOR and an adapter protein regulatory-associated protein of mTOR (raptor)[4,5] (Fig. 1a). Rag dimers are anchored to lysosomes and activated by a lysosome-localized Ragulator adapter complex[6,7], and inactivated by a GATOR1 complex that stimulates the hydrolysis of GTP in active RagA/B-GTP to produce inactive RagA/B-GDP[8,9]. Amino acids, glucose and possibly other nutrients increase the activity of Rags and thereby recruit mTORC1 to lysosomes[4,10,11]. Active Rags also recruit and repress TFEB, a transcription factor that controls the expression of genes needed for lysosome biogenesis and function[12,13]. Once localized at lysosomes, the kinase activity of mTORC1 is regulated by growth factors through a phosphatidylinositol-3-OH kinase (PI3K)–AKT–tuberin (TSC2)–Rheb signalling pathway and other mechanisms[14–17]. Nevertheless, most of the known regulators of mTORC1 are not unique to lysosomes. Only two lysosomal transmembrane proteins, the proton pump v-ATPase and the arginine transporter SLC38A9, have been shown to regulate mTORC1 (refs. [18–21]), suggesting that additional lysosome-specific transmembrane proteins may regulate Rag activity.

Cells with ablated Rags have expanded lysosomes, accumulated autophagosomes and increased expression of TFEB transcriptional targets, but still retain some mTORC1 activity[22–25]. Knockout of two Rag regulators, WDR24 and LAMTOR1, showed similar lysosome and autophagy defects[26,27]. These studies uncovered essential functions of Rags in lysosome/autophagy regulation and point towards other mTORC1 regulators that remain to be identified.

Here, we used a genome-wide short interfering RNA (siRNA) screen to identify additional regulators of lysosomal mTORC1 localization and activity. We identified GPR137B, a lysosome-localized G protein-coupled receptor (GPCR)-like protein with unknown function, as a regulator that promotes the recruitment and activation of mTORC1. We show that GPR137B regulates mTORC1 through Rag proteins by (1) interacting with Rag proteins and increasing the Rag concentration at lysosomes and (2) increasing the GTP-loaded, active state of lysosomal RagA, which causes the recruitment of mTORC1 and an accelerated dissociation of active Rags from lysosomes. We further show that knockout of GPR137B in human cells results in a similar expansion of lysosome compartments and increased autophagy as observed in RagA/B-knockout mouse embryonic fibroblasts (MEFs) and cardiomyocytes[23]. We generated *gpr137ba*-mutant zebrafish and further observed that these animals have some phenotypic similarities to *rraga* (encoding RagA) mutants, including an upregulation of TFEB target genes and an expanded lysosomal compartment phenotype in microglial cells in vivo. Together, our study introduces a GPCR-like activator of lysosomal Rag and mTORC1 signalling that regulates the dynamic exchange of active Rags at lysosomes and provides a potential therapeutic target to regulate mTORC1 activity.

Results

A human siRNA screen identifies a lysosome-localized GPCR-like protein as a regulator of mTORC1. We used 21,041 pools of 4 siRNAs to identify mediators of amino acid signalling to mTORC1 in human fibroblasts (Hs68). Our microscopy-based assay monitored the amino acid-triggered increase in phosphorylation of the ribosomal protein S6 (rpS6) at residue 240 and 244 (refs. [28,29]) (Fig. 1a,b and Supplementary Fig. 1a). The assay captured roughly

[1]Department of Chemical and Systems Biology, Stanford University, Stanford, CA, USA. [2]Department of Developmental Biology, Stanford University, Stanford, CA, USA. [3]Department of Integrative Biology and Physiology and Department of Chemistry and Biochemistry, University of California, Los Angeles, CA, USA. [4]These authors contributed equally: Lin Gan, Akiko Seki. *e-mail: tobias1@stanford.edu

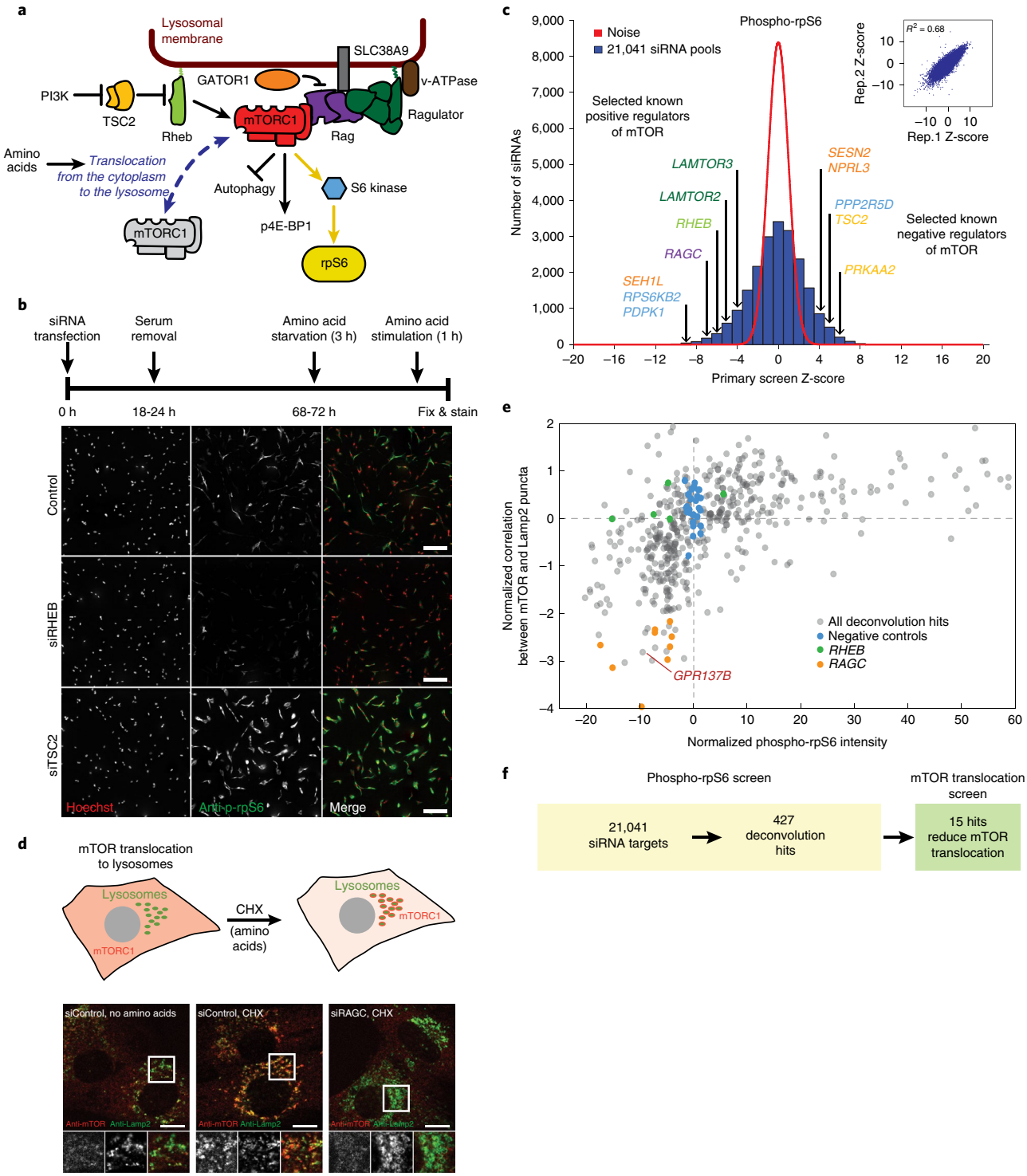


Fig. 1 | A genome-wide siRNA screen in human primary fibroblasts identifies candidate regulators of amino acid-stimulated mTORC1 translocation and activation. a, Schematic representation of the mTORC1 signalling pathway. rpS6 phosphorylation at 240/244 was used as a readout for amino acid-stimulated mTORC1 activation in the siRNA screen. p4E-BP1, phosphorylated 4E-BP1. **b**, siRNA screening strategy (top). Representative immunofluorescence images showing rpS6 phosphorylation at 240/244 in response to amino acid stimulation are also shown (bottom). Knockdown of the genes encoding the mTOR pathway components Rheb and TSC2 are shown as examples for increased and decreased rpS6 phosphorylation, respectively. Scale bars, 200 µm. **c**, The genome-wide screen identifies siRNA pools (four individual siRNAs targeting the same gene) that increase or decrease rpS6 phosphorylation. Z-scores of 21,041 siRNA pools are plotted over a normally distributed noise distribution. The inset shows the reproducibility of Z-scores of two replicate (rep.) sets, calculated by linear regression. The labelled genes show known mTOR pathway regulators, colour coded according to the schematic in **a**. **d**, Microscopy-based mTORC1 translocation assay based on automated correlation between mTOR and Lamp2 images. Confocal images of Hs68 fibroblasts co-stained for endogenous Lamp2 and mTOR. CHX, cycloheximide. Scale bars, 10 µm. Dashed grey lines mark control cells without siRNA perturbation. **e**, Lysosome translocation screen identifies candidate siRNAs that decrease mTOR localization to lysosomes as well as rpS6 phosphorylation. **f**, Sequential selection strategy for candidate regulatory genes (see Methods). Experiments in **b** and **d** were repeated independently 12 and 5 times respectively, as controls for each run of the screen.

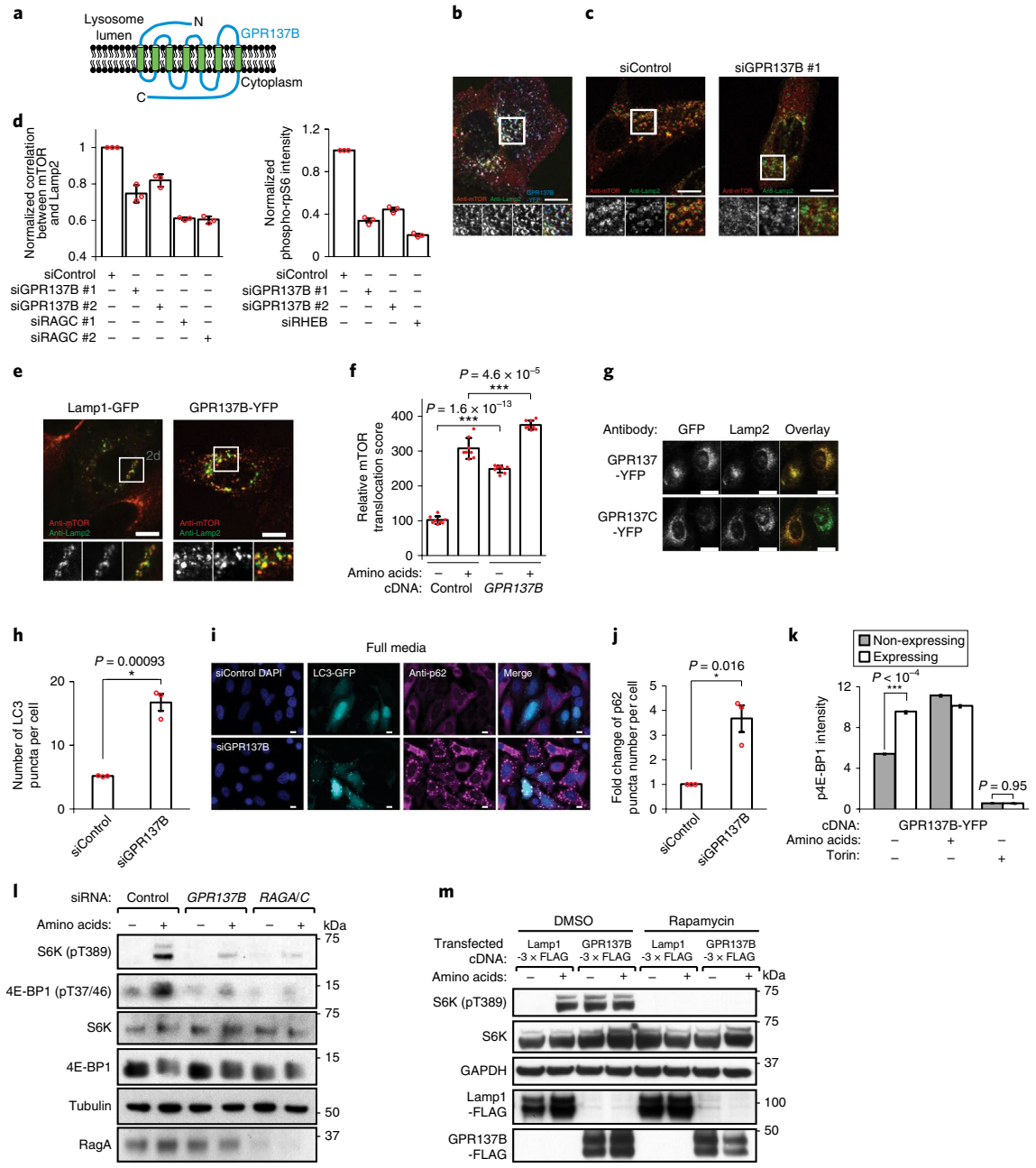


Fig. 2 | GPR137B regulates mTORC1 translocation to lysosomes and mTORC1 activation. a, Predicted transmembrane domains of GPR137B. **b**, Confocal images of expressed GPR137B-YFP, the lysosome marker Lamp2 and mTOR in Hs68 cells. **c**, siRNA knockdown of *GPR137B* reduces amino acid-induced mTOR translocation. **d**, Analysis of mTOR and Lamp2 colocalization and rpS6 phosphorylation for siRNAs targeting *GPR137B*, *RHEB* and *RAGC*. Error bars indicate ±s.d. of the mean; $n = 3$ independent experiments. **e**, Confocal images of HeLa cells showing increased amino acid-induced mTOR translocation in cells expressing GPR137B-YFP or Lamp1-GFP as control. **f**, Binary mask analysis showing that amino acid-triggered increase in mTOR localization at lysosomes is regulated by GPR137B-YFP overexpression. Error bars indicate ±s.d. of the mean; $n = 8$ independent experiments; $P = 1.6 \times 10^{-13}$ (two-tailed Student's *t*-test). **g**, Lysosomal localization of GPR137-YFP and GPR137C-YFP (HeLa cells). **h**, siRNA knockdown of *GPR137B* enhances autophagy as measured by LC3-GFP. Error bars indicate ±s.d. of the mean; $n = 3$ independent experiments (two-tailed Student's *t*-test). **i**,**j**, siRNA knockdown of *GPR137B* causes autophagy flux defects as measured by p62 staining (**i**) and the fold change of p62 puncta number (**j**). Scale bar, 20 µm. Error bars indicate ±s.d. of the mean (*P* value was calculated by a ratio paired, two-tailed Student's *t*-test; $n = 3$ independent experiments). **k**, GPR137B-YFP expression causes phosphorylation of 4E-BP1 during amino acid starvation. Error bars indicate ±standard error of the mean (s.e.m.) of the mean (*P* values, comparison of transfected, $n = 2{,}329$ cells for no amino acids, $n = 2{,}211$ cells for plus amino acids and $n = 2{,}308$ cells for Torin; to untransfected cells, $n = 3{,}256$ cells for no amino acids, $n = 3{,}099$ cells for plus amino acids and $n = 3{,}048$ cells for Torin; two-tailed Student's *t*-test). **l**, Knockdown of *GPR137B* inhibits amino acid-induced S6K and 4E-EP1 phosphorylation. HEK293T cells transfected with siControl, siGPR137B or siRAGA/C were starved of amino acids for 1 h and stimulated with or without amino acids for 30 min. Western blot analysis of phosphorylation of S6K and 4E-BP1 is shown. **m**, Same as panel **l** but with transiently transfected GPR137B-3×FLAG or Lamp1-3×FLAG. Amino acid starvation occurred for 3 h and amino acid re-addition for 30 min with or without rapamycin. DMSO, dimethylsulfoxide. Results in **b**, **c** and **g** were confirmed by three independent experiments and by two independent experiments in **l** and **m**. In all figures, $^{*}P = 0.01$–0.05; $^{**}P = 0.001$–0.1, $^{***}P < 0.001$. All scale bars are 10 µm except when noted.

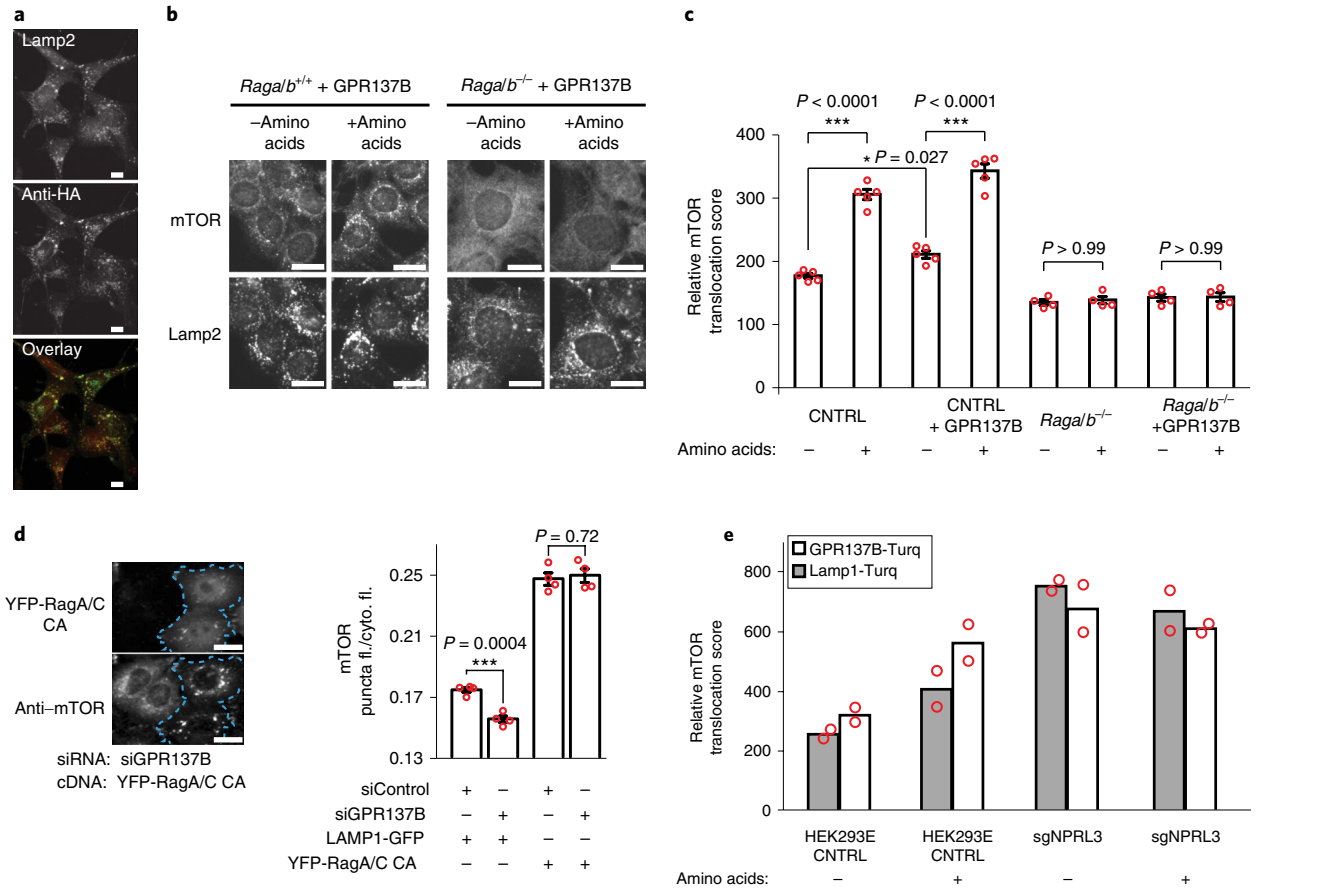


Fig. 3 | GPR137B regulates mTORC1 through RagA/B. a, Stable expression of GPR137B-HA in *Rraga/b*$^{-/-}$ MEFs visualized by staining for HA and Lamp2. Scale bars, 20 µm. The experiment was performed twice. **b**, mTOR translocation could not be rescued in *Rraga/b*$^{-/-}$ MEFs by stable expression of GPR137B. MEFs starved of amino acids for 60 min and restimulated with amino acids for 10 min were stained for mTOR and Lamp2. Scale bars, 20 µm. **c**, Quantification of mTOR translocation in *Rraga/b*$^{+/+}$ (control (CNTRL)) and *Rraga/b*$^{-/-}$ MEFs either stably expressing GPR137B or not stably expressing GPR137B. Error bars are ±s.d. of the population average and one-way ANOVA analysis followed by Tukey's test shows that there is significance among control groups with or without GPR137B, but not among *Rraga/b*$^{-/-}$ MEFs with or without GPR137B; $n = 4$ independent experiments. **d**, Expression of the constitutively active RagA/C heterodimer (RagA Q66L/RagC T75N) rescued mTOR translocation in cells treated with siGPR137B. The left panel shows HeLa cells transfected with siGPR137B and RagA Q66L/RagC T75N (YFP-RagA/C CA) and then stained for mTOR. Cells co-expressing YFP-RagA/C CA are marked by blue dashed lines. The right panel shows an analysis of the effects on mTOR translocation by Lamp1-GFP or YFP-RagA/C CA expression in cells treated with siGPR137B versus siControl. Error bars are ±s.d. of the population average and the *P* value was calculated using a two-tailed Student's *t*-test; $n = 4$ independent experiments Scale bars, 20 µm. Cyto, cytoplasm. fl, fluorescence. **e**, GPR137B does not induce additional mTOR translocation in *NPRL3*$^{-/-}$ HEK293E cells that have constitutively active RagA. Parental HEK293E cells or *NPRL3*$^{-/-}$ cells transfected with either Lamp1-Turquoise (Turq) or GPR137B-Turquoise were treated as in **a**. The mean from $n = 2$ independent experiments is plotted. $^{*}P < 0.05$; $^{***}P < 0.001$.

an equal number of 1,000 siRNA pools that target positive and negative regulators (Fig. 1c, Supplementary Fig. 1b and Supplementary Table 1), such as the known mTORC1 activator Rheb and the suppressor TSC2 (Fig. 1c, arrows). We confirmed the screening results using individual siRNAs and narrowed our focus on 427 high-confidence candidates (Supplementary Fig. 1c). Ingenuity pathway analysis showed that genes associated with insulin–growth factor, PI3K–AKT, extracellular signal-regulated kinase (ERK)–mitogen-activated protein kinase (MAPK), Hedgehog, p53, 5′-AMP-activated protein kinase (AMPK), the glycine cleavage pathway and cell-cycle signalling pathways were significantly enriched in the set (Supplementary Fig. 1d and Supplementary Table 2).

As amino acid-induced translocation of mTORC1 to lysosomes is a key step in the activation process[6,8], we used automated microscopy to monitor mTORC1 translocation by quantifying the colocalization between the lysosome marker lysosome-associated membrane glycoprotein 2 (Lamp2) and mTOR. To exclude indirect regulators that control amino acid uptake, we starved cells and then induced a transient increase in intracellular amino acids by inhibiting protein translation using cycloheximide[30] (Fig. 1d and Supplementary Fig. 1e). Using this assay, we screened for effects caused by the knockdown of each of the 427 candidate genes. A small subset of hits significantly reduced mTOR translocation to lysosomes as well as rpS6 phosphorylation (Fig. 1e,f), consistent with the interpretation that only some genes regulate the translocation of mTORC1, whereas most genes regulate mTORC1 activity after lysosome translocation. Supplementary Table 3 shows a rank-ordered list of 15 identified genes. RagC was the top hit regulating mTOR translocation in the screen, followed by less-characterized candidate genes that include transporters, the anti-apoptotic factor TIAF1 and a F-box DNA helicase, suggesting that mTORC1 translocation is regulated by nutrient, metabolism and stress pathways. We focused our subsequent analysis on GPR137B, because it is localized to the lysosome[31] and because it is a predicted seven-transmembrane protein with a low sequence homology to GPCRs (Fig. 2a).

GPR137B regulates lysosomal localization and activity of mTORC1. Consistent with a reported lysosomal localization[31], we found that GPR137B-yellow fluorescent protein (YFP) colocalized with the lysosomal marker Lamp2 and with mTOR after amino acid stimulation (Fig. 2b). We quantified the relative lysosomal localization of mTOR using a colocalization score or automated analysis of mTOR localization based on a binary lysosome mask (Supplementary Note). Independent siRNAs in two cell types (Hs68 and HeLa cells) confirmed the screening result (Fig. 2c,d and Supplementary Fig. 2a–c). Time-course analysis of rpS6 phosphorylation revealed that *GPR137B* knockdown reduces basal mTORC1 activity in nutrient-replete cells as well as mTORC1 reactivation in nutrient-stimulated cells (Supplementary Fig. 2d). Furthermore, overexpression of GPR137B increased mTOR translocation weakly in the presence of amino acids and strongly in the absence of amino acids (Fig. 2e,f and Supplementary Fig. 2e). Finally, *GPR137* and *GPR137C*, two genes homologous to *GPR137B*, probably have a similar role in regulating mTORC1 as we found that they were also localized to the lysosome (Fig. 2g) and both increased mTOR translocation to lysosomes when overexpressed (Supplementary Fig. 2f,g). Together, these results suggest that GPR137B is part of a family of lysosome-localized GPCR-like proteins that regulate mTORC1 translocation to lysosomes.

An important role of mTORC1 is to inhibit autophagosome formation through phosphorylation of the ULK1–mATG13–FIP200 complex[32]. Consistent with a role of GPR137B in regulating mTORC1 activity, knocking down *GPR137B* increased autophagy, as indicated by an increase in the number of LC3-GFP puncta per cell (Fig. 2h). p62 (also known as SQSTM1) is an ubiquitin-binding protein that is degraded by autophagy and accumulates if autophagy flux is reduced or defective[10,23,25,27,33]. We observed a marked upregulation of p62 in *GPR137B*-knockdown cells, and the larger, brighter p62 and LC3-GFP puncta observed mostly in GPR137B-depleted cells colocalized with each other (Fig. 2i,j), suggesting that autophagy flux defects contribute to the LC3 phenotype in *GPR137B*-knockdown cells.

The translational regulators eukaryotic translation initiation factor 4E-binding protein 1 (4E-BP1) and S6 kinase (S6K) are critical mTORC1 substrates and regulators of protein synthesis and cell size[34–36]. Overexpression of GPR137B-YFP in cells starved of amino acids increased the phosphorylation of 4E-BP1 close to the level reached by amino acid stimulation (Fig. 2k and Supplementary Fig. 2h for controls). Furthermore, biochemical analysis confirmed that knockdown of *GPR137B* suppresses the phosphorylation of S6K and 4E-BP1 (Fig. 2l), and the GPR137B expression-mediated increase in S6K and 4E-BP1 phosphorylation was abolished following rapamycin treatment (Fig. 2m). Finally, GPR137B mediates its effects on S6K through amino acid signalling rather than growth factor regulation of mTORC1 (Supplementary Fig. 2i,j). Thus, GPR137B regulates amino acid-induced mTORC1 translocation to lysosomes and mTORC1 activity, and probably has a functional role in regulating autophagy as well as protein synthesis and cell size through the regulation of S6K, 4E-BP1 and other mTORC1 targets.

GPR137B regulates mTORC1 localization and activity through Rag GTPases. Several lines of evidence argue that GPR137B regulates mTORC1 localization and activity through Rags. First, we used RagA/B-knockout MEFs[23] and found that stable expression of GPR137B in these cells could not restore mTORC1 translocation (Fig. 3a–c and Supplementary Fig. 3a). Second, when we overexpressed constitutively active RagA/C (RagA Q66L and RagC T75N)[4] in HeLa cells, knockdown of *GPR137B* did not alter the increased lysosomal mTORC1 localization (Fig. 3d). In an independent strategy to activate endogenous Rags, we overexpressed GPR137B in HEK293E cells deficient for the GATOR1 component NPRL3 (refs. [8,37]) that have constitutively active RagA. Whereas the wild-type cells showed a GPR137B expression-mediated increase in mTORC1 translocation, GPR137B did not cause additional mTORC1 translocation in the knockout cells (Fig. 3e). Together, these results suggest that GPR137B signals through Rag GTPases to regulate mTORC1 translocation and activity.

GPR137B interacts with Rags and increases the lysosomal localization of RagA. We next evaluated the binding interactions of GPR137B with known components of the mTORC1 regulatory machinery. In HEK293T cells, we found that GPR137B co-immunoprecipitated with mTOR, raptor and RagA (Fig. 4a and Supplementary Fig. 3b). Control experiments using the unrelated lysosomal transmembrane protein NPC intracellular cholesterol transporter 1 (NPC1) as well as tests using other mTORC1 regulators are shown in Supplementary Fig. 4a,b.

Interestingly, when we co-expressed two GPR137B constructs with different tags, we observed an apparent amino acid-stimulated interaction of GPR137B with itself that is dependent on the presence of Rags (Fig. 4b), suggesting that more than one GPR137B protein is part of an amino acid-regulated lysosomal signalling complex. Experiments using RagA/B-knockout MEFs suggest that this amino acid-regulated self-interaction of GPR137B proteins does not require Rag activity, suggesting a possible direct or indirect regulation of GPR137B by amino acids (Fig. 4c and Supplementary Fig. 4c). Notably, the interaction between GPR137B and RagA was not amino acid sensitive (Fig. 4a and Supplementary Fig. 4d).

It has recently been reported that Sestrin2 functions as a leucine sensor[37–41]. We used Sestrin1/2/3 triple-knockout cells[37] that have increased basal lysosomal localization of mTORC1. However, overexpression of GPR137B could further increase mTOR translocation to lysosomes in these cells (Supplementary Fig. 4e), arguing that GPR137B can regulate Rag and mTORC1 independent of the Sestrins. Thus, we did not further investigate this regulatory pathway.

We next tested whether GPR137B regulates the localization of Rags analogous to Ragulator proteins that anchor Rags to lysosomes. Markedly, increased GPR137B expression did not only increase mTOR translocation but also caused a small but significant increase in RagA localization at lysosomes (Fig. 4d; see Supplementary Fig. 4f for RagC data), whereas siRNA against *GPR137B* reduced lysosomal RagA (Fig. 4e) and RagC (Fig. 4f) localization. Knockdown of the Ragulator component *LAMTOR2* is included for comparison. When Ragulator expression was reduced, GPR137B did not significantly increase Rag recruitment or mTORC1 activity, and co-expressing GPR137B did not rescue the reduced RagA lysosomal localization (Supplementary Fig. 4g,h). Thus, GPR137B interacts with Rags and increases lysosomal Rag localization in a Ragulator-dependent manner. Taken together with our data in Fig. 3, the binding and localization results suggest that GPR137B regulates Rag localization and possibly RagA-GTP loading and activity.

GPR137B increases Rag activity to recruit mTORC1. We used the selective binding of mTORC1 to RagA-GTP over RagA-GDP as a measure to determine whether RagA is in the active GTP-bound state[4]. Consistent with a role of GPR137B in regulating RagA-GTP loading, knockdown of *GPR137B* inhibits the amino acid-induced interaction between RagA and both mTOR and raptor (Fig. 5a and Supplementary Fig. 5a,b), whereas overexpression of GPR137B increases the interaction between them (Fig. 5b and Supplementary Fig. 5c,d). Markedly, at high GPR137B expression levels, the binding of RagA and raptor is increased even in the absence of amino acids, suggesting that overexpression of GPR137B can increase RagA-GTP loading even in the absence of amino acids (Fig. 5b and Supplementary Fig. 5c,d).

We next determined whether co-expression of Rag and GPR137B induces synergistic mTORC1 translocation. When we co-expressed

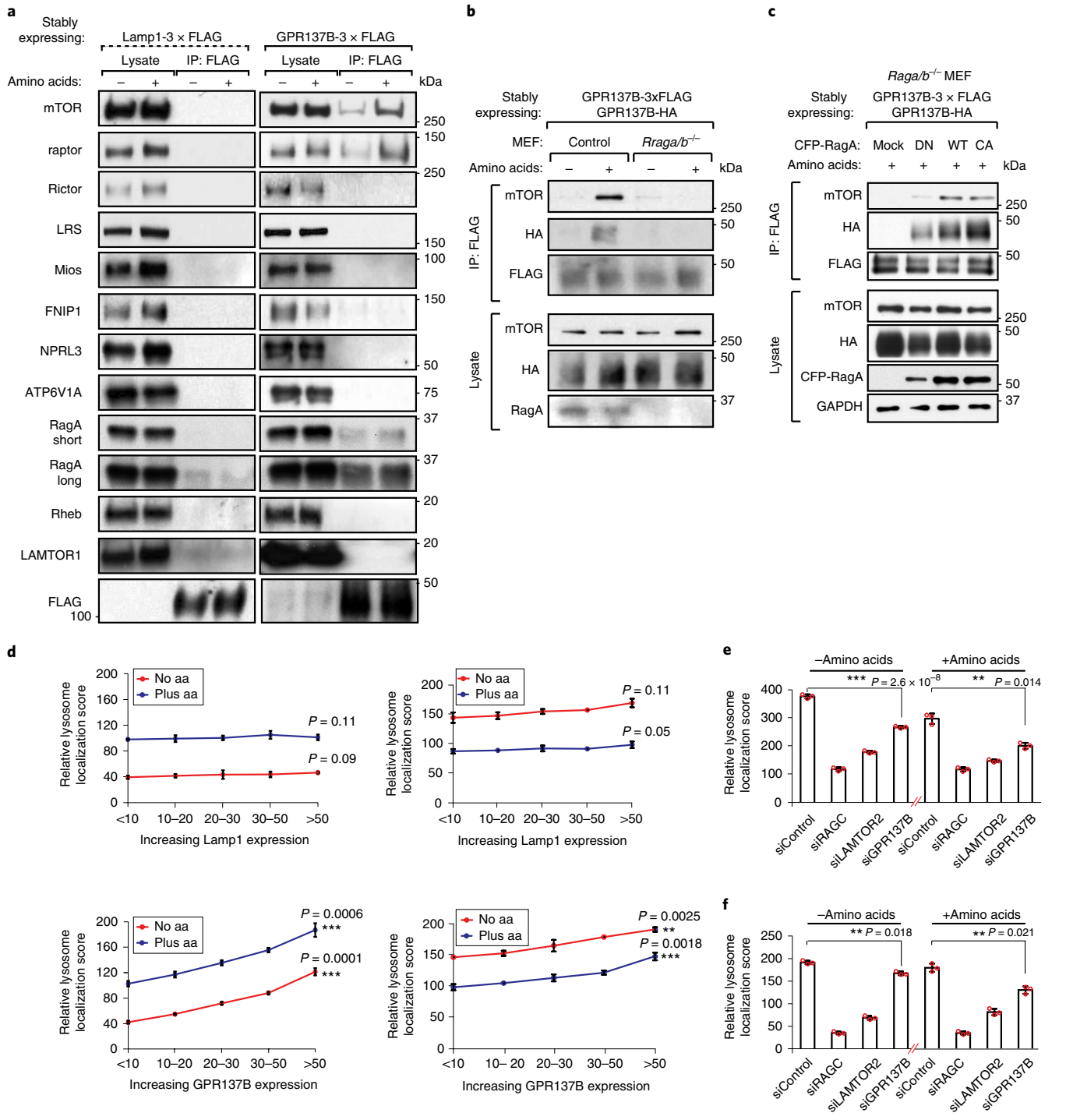


Fig. 4 | GPR137B forms an amino acid-sensitive complex with mTORC1 through Rag GTPases and binds to RagA constitutively as an adaptor for lysosomal localization. a, Amino acid-regulated interaction of GPR137B with mTOR, raptor and RagA. HEK293T cells were stably expressing Lamp1-3×FLAG or GPR137B-3×FLAG, starved of amino acids for 2 h and stimulated for 10 min. IP, immunoprecipitation. **b**, Rag GTPases are necessary for the GPR137B–mTOR interaction, and evidence of self-interaction between GPR137Bs is shown. GPR137B-3×FLAG and GPR137B-HA were stably expressed in control or *Rraga/b*$^{-/-}$ MEFs. **c**, RagA overexpression restores GPR137B self-interaction regardless of RagA-GTP loading. RagA DN(T21N), wild type (WT) or CA(Q66L) mutants were expressed in *Rraga/b*$^{-/-}$ MEFs. Cells were amino acid starved for 4 h then stimulated for 20 min. For **a**–**c**, $n = 2$ independent experiments. **d**, Amino acid (aa) stimulation reduces lysosomal localization of RagA, and GPR137B increases RagA localization at lysosomes. Increasing the expression of GPR137B causes a gradual increase in the lysosomal localization of mTOR (left panels), as well as of RagA (right panels). Amino acid-starved or restimulated HeLa cells expressing either Lamp1-Turquoise or GPR137B-Turquoise were stained for endogenous mTOR or RagA and Lamp2 and binned for different levels of Turquoise expression. The median value for each bin is plotted as the mean of triplicates ± s.d. from three independent experiments. Repeated-measures one-way ANOVA analysis followed by Tukey's test shows significant differences among different expression bins of GPR137B but not of Lamp1. **e**,**f**, Knockdown of *GPR137B* decreases lysosomal localization of RagA (**e**) and of RagC (**f**) in amino acid-starved and restimulated HeLa cells. Two-tailed, Student's *t*-test shows significant difference between control and siGPR137B; $^{**}P < 0.01$ and $^{***}P < 0.001$. Mean ± s.d. is plotted from $n = 3$ independent experiments.

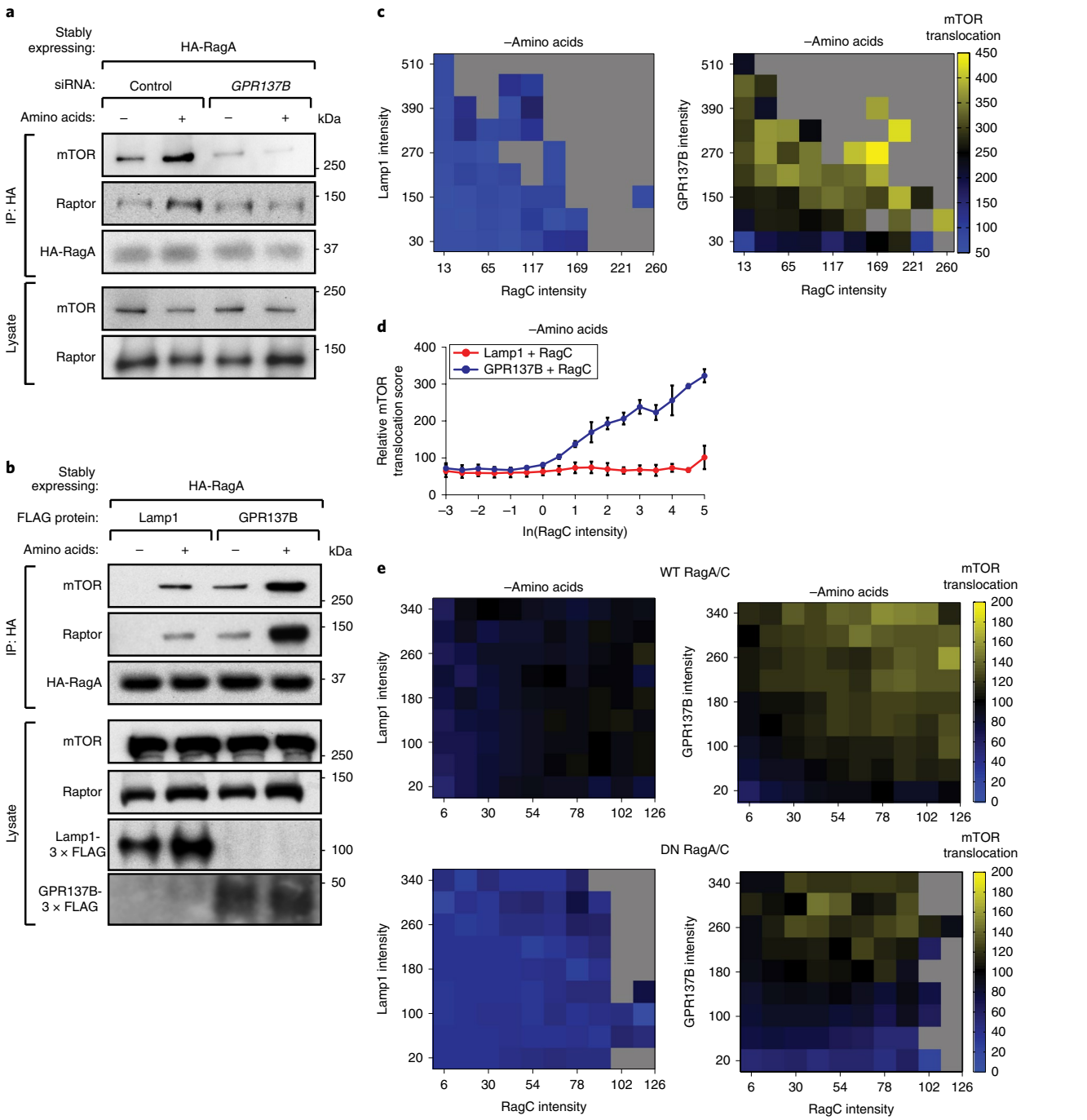


Fig. 5 | Evidence that GPR137B can activate RagA/C even in the absence of amino acids. a, mTORC1 interaction with HA-RagA was markedly reduced in cells treated with siGPR137B. *GPR137B* was knocked down in HEK293T cells stably expressing HA-RagA. HA-RagA was immunoprecipitated and the interaction with endogenous mTORC1 subunits was detected by western blot. **b**, mTORC1 interaction with HA-RagA was increased in GPR137B-overexpressing cells. GPR137B was transiently overexpressed in HEK293T cells stably expressing HA-RagA. In **a** and **b**, the cells were starved of amino acids for 2 h and then treated with starvation or amino acid-containing media for 10 min. Cells were then treated with a cell-permeable chemical crosslinker (DSP) and subjected to HA immunoprecipitation. $n = 2$ independent experiments in **a** and **b**. **c**, Analysis of synergism between GPR137B and Rags for mTORC1 activation. GPR137B co-expression with RagC promotes Rag expression-dependent recruitment of mTORC1 during amino acid starvation (10–12 h). Control heatmap experiments show that co-expression of Lamp1 with RagC does not induce mTORC1 translocation at any expression level of Lamp1 or RagC (left), but co-expression of GPR137B with RagC causes synergistic mTORC1 translocation at even low levels of RagC expression in the absence of amino acids (right). Heatmaps are plotted from translocation scores pooled from three independent experiments. **d**, Synergy analysis as in **c** comparing GPR137B-expressing and control Lamp1-expressing cells. There is a sharp expression dependence of mTORC1 translocation on RagC expression only when co-expressed with GPR137B. Data represent mean ± s.d.; $n = 3$ independent experiments. **e**, GPR137B co-expression with wild-type RagA/C in *Rraga/b*$^{-/-}$ MEFs promotes RagA/C expression-dependent mTORC1 translocation in the absence of amino acids, and this effect is significantly lower in *Rraga/b*$^{-/-}$ MEFs co-expressing GPR137B and DN RagA/C (RagA T21L/RagC Q120L). *Rraga/b*$^{-/-}$ MEFs transiently expressing either Lamp1 as control or GPR137B, along with wild-type or DN RagA/C proteins, were starved for 2 h, fixed and stained for mTOR and Lamp2. In **c**–**e**, RagC expression is used as a readout of RagA/C dimer expression.

RagC[42] together with Lamp1 control, mTORC1 translocation did not significantly increase, suggesting that Rags, at any level, mediate only minimal basal mTORC1 recruitment when amino acids are low (Fig. 5c,d). By contrast, we found synergistic recruitment of mTORC1 when we co-expressed Rag together with GPR137B (Fig. 5c, right panel, Fig. 5d, blue line, and Supplementary Fig. 6a). The strong synergy between GPR137B and Rag expression on mTOR translocation is consistent with a direct regulation of Rags by GPR137B.

To further investigate whether GPR137B causes mTORC1 translocation through promoting Rag-GTP loading, we co-expressed GPR137B with wild-type or dominant negative (DN) RagA/C (RagA T21L/RagC Q120L) in *Rraga/b*-null MEFs. These RagA/B-knockout cells had no mTORC1 translocation when stably expressing GPR137B alone (Fig. 3b,c), and minimal rescue of mTORC1 translocation when transiently co-expressing wild-type or DN RagA/C and Lamp1. By contrast, we observed robust mTORC1 translocation even in the absence of amino acids when we co-expressed GPR137B and wild-type RagA/C, but significantly lower translocation when we co-expressed DN RagA/C (Fig. 5e and Supplementary Fig. 6b–d). These results support the hypothesis that the level of GPR137B regulates RagA-GTP loading and activity.

Photobleaching recovery analysis suggests that GPR137B regulates a cycle of dynamic activation and dissociation of lysosomal Rags. Figure 4d also revealed an unexpected amino acid-triggered reduction in Rag localization at lysosomes. When we compared the kinetics of Rag and mTOR localization, we found that endogenous RagA and RagC dissociated from lysosomes in response to amino acids with kinetics that paralleled the increase in mTOR translocation to lysosomes (Fig. 6a–c). We next made use of previous studies that showed a negative feedback in which mTORC1-mediated Rag ubiquitylation reduces lysosomal localization of mTORC1 after amino acid stimulation[43,44]. Indeed, when we treated amino acid-stimulated cells with rapamycin to inhibit the activity of mTORC1, more mTOR translocated to lysosomes and a greater fraction of RagA and RagC dissociated from lysosomes (Fig. 6d–f). The anti-correlated kinetics and amplitude of mTOR and Rag localization suggest that the recruitment of mTORC1 and the dissociation of Rags are connected events.

We next used fluorescence photobleaching recovery analysis to test whether GTP loading of RagA accelerates dissociation of RagA/C from lysosomes. In cells overexpressing fluorescently tagged wild-type RagC and DN RagA, the RagC dissociation rate was slower than in cells co-expressing wild-type RagC and constitutively active (CA) RagA (Fig. 6g,h). This suggests that GTP loading of RagA lowers the affinity of RagA/C for lysosomes and accelerates RagA/C dissociation. Indeed, lysosomal RagC dissociated more rapidly after amino acid stimulation, which increased GTP loading of RagA (Fig. 6i). These results are consistent with a recent publication showing Rags cycle on and off the lysosomes depending on their activation state[45]. When we expressed GPR137B in amino acid-starved cells, we found a small but significant increase in RagC dissociation (Fig. 6j,k). Conversely, when we knocked down GPR137B, there was a small but significant decrease in the RagC exchange rate (Fig. 6l,m). When we expressed GPR137B in *NPRL3*$^{-/-}$ HEK293E cells where Rags are mostly GTP loaded[8], there was no significant difference in the RagC exchange rate from control cells (Supplementary Fig. 6e,f). Taken together, these results suggest that GPR137B accelerates Rag dissociation from the lysosome through RagA-GTP loading.

Together with previous studies that showed mTORC1 can be active at different cellular locations[46,47], these results suggest that GPR137B regulates Rags in three steps: first, by increasing RagA levels at the lysosomes; second, by promoting the activation of lysosomal RagA, which recruits mTORC1 to the lysosomes for a limited time period; and third, by promoting Rag dissociation from the lysosomes possibly as an active or activatable cytosolic Rag–mTORC1 complex.

To directly test whether RagC and the mTORC1 subunit raptor can remain bound to each other in the cytoplasm, we co-expressed RagC with a conjugated C1 domain from rat protein kinase C-γ (PKC-γ)[48] along with fluorescently tagged raptor, CA RagA and a membrane marker in HEK293T cells. In this in vivo binding assay, a phorbolester (phorbol myristate acetate (PMA)) was used to rapidly recruit cytosolic C1-conjugated RagC to the plasma membrane and monitor how much of the putative binding partner raptor is pulled along. Indeed, we observed a concomitant recruitment of raptor (Fig. 7a–c and Supplementary Fig. 7a,b), arguing that Rags and the mTORC1 subunit raptor can be bound to each other in the cytoplasm. Given the finding that inactive Rags do not bind to raptor[4,49], and active Rag dissociates from the lysosomes along with mTOR[45], our results suggest that active Rag–mTORC1 complexes diffuse in the cytoplasm after dissociation and that Rag–mTORC1 remains in an active state until Rag is inactivated.

Mutational analysis in human cells and zebrafish provides evidence that GPR137B regulates lysosomal morphology through Rag. Both GPR137B-knockout and GPR137-knockout HAP1 cells showed an expanded lysosomal compartment as measured by larger LysoTracker green-positive puncta (Fig. 8a,b), as well as an increased number of autophagosomes and/or autolysosomes as measured by increased LC3B puncta per cell (Fig. 8c), similar to Rag or Rag regulator knockouts[23,26,27]. In addition, in both cell lines, the lysosomal localization of endogenous RagA was decreased, similar to the *GPR137B* knockdown result (Fig. 8e). Nevertheless, mTORC1 translocation to lysosomes was still regulated by amino acids in both knockout cell lines (Fig. 8d and Supplementary Fig. 8a).

To investigate the function of GPR137B in vivo, we focused on four homologues of *GPR137B* in zebrafish: *gpr137ba*, *gpr137bb*, *gpr137c* and *gpr137*. Of these, Gpr137ba is most similar to the human GPR137B protein (Supplementary Fig. 8b,c). The hypothesis that GPR137B activates RagA predicts that there should be phenotypic similarities between *rraga* mutants and mutants in one or more of the four *gpr137* genes. We generated mutants for three of the annotated genes, *gpr137ba*, *gpr137c* and *gpr137*, using transcription activator-like effector nuclease (TALEN)-targeting nucleases (Supplementary Fig. 8d). *gpr137bb* was annotated more recently and we have analysed its function in transient clustered regularly interspaced short palindromic repeats (CRISPR) experiments. Our preliminary studies revealed similarities between mutants for *rraga* and *gpr137ba*, but not *gpr137c* or *gpr137* mutants, or wild-type fish injected with CRISPR-associated protein 9 (Cas9) and guide RNA for *gpr137bb*. Thus, we focused additional analyses on the *gpr137ba* mutants.

Zebrafish *rraga* mutants have abnormal microglia with expanded lysosomes[25], so we examined these specialized brain macrophages in *gpr137ba*-mutant zebrafish. Microglia in *gpr137ba* mutants had an expansion of the lysosomal compartment, with large clusters of LysoTracker red-positive puncta, similar to *rraga*-mutant zebrafish (Fig. 8h,i). Homozygous *gpr137ba*-mutant fish had otherwise normal morphology and were viable as adults (Supplementary Fig. 8e). Microglial cell numbers and markers of autophagy, such as LC3B and p62, were unchanged in *gpr137ba* mutants relative to controls (Fig. 8f,g and Supplementary Fig. 8f).

RagA represses the activity of the key lysosomal transcription factor TFEB[50], and quantitative real-time PCR studies in zebrafish have demonstrated that transcripts of some TFEB targets are significantly upregulated in *rraga*-mutant zebrafish[25,51]. The hypothesis that GPR137B activates RagA predicts that TFEB targets will be similarly upregulated in *gpr137ba* mutants. To investigate this possibility, we conducted quantitative real-time PCR on larvae from a

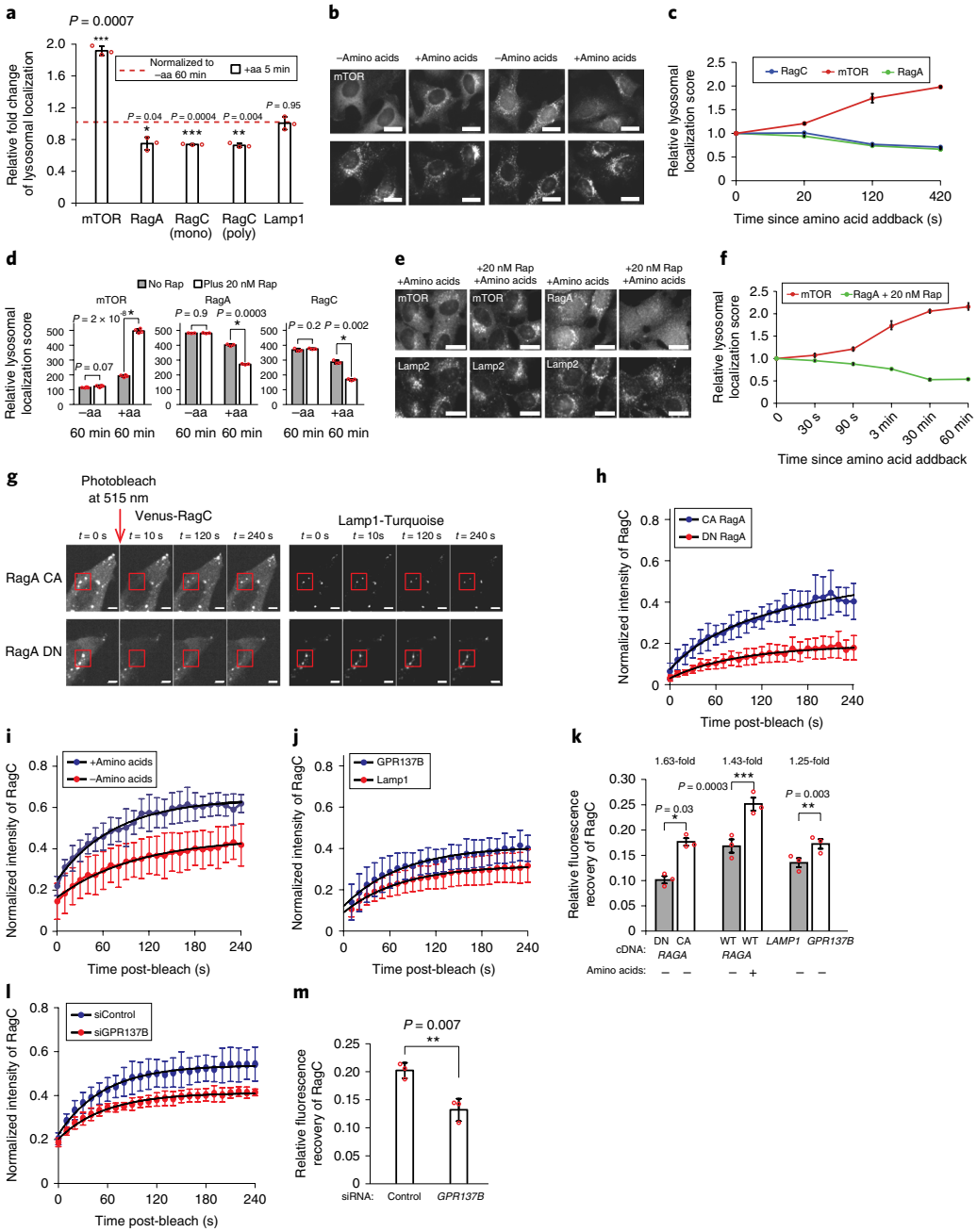


Fig. 6 | Evaluation of the role of GPR137B in regulating Rags by monitoring changes in the exchange rate of RagA/C from lysosomes. a, Endogenous RagA/C dissociates from lysosomes following amino acid stimulation (HeLa cells). Colocalization analysis as in Fig. 2. Data are mean ± s.d.; $n = 3$ independent experiments (P values were calculated using a two-tailed Student's t-test). **b**, Representative images of mTOR and RagA staining as in **a**. Scale bars, 20 µm. **c**, RagA and RagC dissociate from lysosomes with kinetics anti-correlated with mTOR translocation. Stained as in **a**. Data are mean ± s.d.; $n = 3$ independent experiments. **d**, Rapamycin (Rap) increases the lysosomal retention of mTOR and accelerates dissociation of RagA and RagC. Stained as in **a** (mean ± s.d.; $n = 3$ independent experiments; P values were determined by a two-tailed Student's t-test). **e**, Representative images of endogenous mTOR and RagA, stained as in **a**. Scale bars, 20 µm. **f**, Endogenous RagA dissociates from lysosomes with kinetics anti-correlated with mTOR translocation (with rapamycin), stained as in **a**. Data are mean ± s.d.; $n = 3$ independent experiments. **g**, Photobleaching recovery measurements of RagC exchange. Lysosome-localized, Rag CA increases the exchange rate of bleached Venus-RagC from lysosomes. RagA CA (HA GST RagA66L) (top) or RagA DN (HA GST RagA21L) (bottom) paired with wild-type Venus-RagC before (frame 1) and after photobleaching (frames 2–4). The red boxes denote the lysosomes. Ten-second time points, confocal microscope at ×40. Scale bars, 5 µm. **h**, Averaged photobleaching recovery curves ± s.d. for RagA CA ($n = 6$ cells) and RagA DN ($n = 7$ cells). **i**, Lysosomal Venus-RagC intensity recovers faster with than without amino acids. $n = 10$ cells each. **j**, Lysosomal Venus-RagC intensity recovers faster when co-expressed with GPR137B than with Lamp1 as control. Lamp1: $n = 9$ cells; GPR137B: $n = 7$ cells. In **h**–**j**, error bars indicate ±s.d. of the mean and intensities are normalized to the intensity before photobleaching. **k**, Bar graph representation of data in **h**–**j**. $n = 3$ independent experiments; data are mean ± s.d. (P values were determined by two-tailed Student's t-test). **l**,**m**, Lysosomal Venus-RagC intensity recovers slower in cells treated with siGPR137B than in cells treated with siControl (**l**). siControl: $n = 9$ cells; siGPR137B: $n = 9$ cells. A bar graph representation of data in **l** is also shown (**m**). $n = 3$ independent experiments; data represent mean ± s.d. (P values were determined by two-tailed Student's t-test; $^*P < 0.05$, $^{**}P < 0.01$ and $^{***}P < 0.001$).

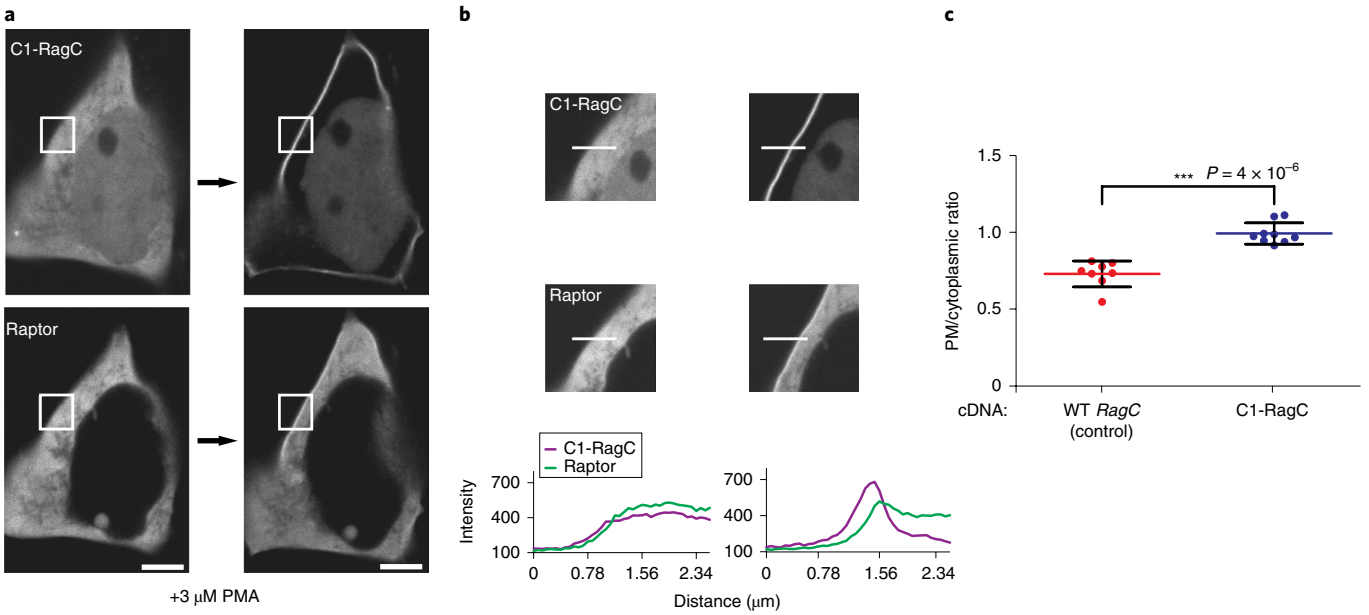


Fig. 7 | Active Rag and raptor can rapidly diffuse in the cytoplasm while being in a complex. a, Raptor translocates to the plasma membrane along with C1-domain-tagged RagC following the addition of PMA. Images are of HEK293T cells transiently transfected with YFP-raptor, C1-mRuby-RagC and HA-CA RagA (RagA Q66L) before and after 3 uM PMA. The white boxes correspond to the magnified images in **b**. Scale bars, 5 μm. **b**, Magnified images of raptor and C1-RagC translocation to the plasma membrane (top) and line scan profiles measuring the intensities across the plasma membrane edge (bottom). The white lines indicate the positions of the line scan profiles. **c**, Quantification of the plasma membrane/cytoplasmic intensity ratio of YFP-raptor in cells expressing either wild-type RagC ($n = 8$) or C1-RagC ($n = 9$), along with YFP-raptor, HA-CA RagA and iRFP-CAAX. Only low YFP-raptor-expressing cells were analysed. $n = 3$ independent experiments; data represent mean ± s.d.; the P value was calculated from a two-tailed Student's t-test; $^{***}P < 0.001$.

cross of *gpr137c*$^{+/-}$; *gpr137*$^{+/-}$; *gpr137ba*$^{-/-}$ × *gpr137c*$^{-/-}$; *gpr137*$^{+/-}$; *gpr137ba*$^{+/-}$ adults. Individual fish were genotyped for the *gpr137ba* mutation and pooled, so that one pool of siblings was *gpr137ba*$^{-/-}$, whereas the other pool was *gpr137ba*$^{+/-}$; mutations in the other genes were randomly segregated between both pools. Quantitative PCR analysis revealed that some TFEB target genes were significantly upregulated in the *gpr137ba*-mutant pool compared to the control pool (Fig. 8j), providing evidence that *gpr137ba*, similar to *rraga*, represses the activity of TFEB. Although the levels of p62 protein were similar in immunoblot analysis (Supplementary Fig. 8f), *p62 (sqstm1)* is one of the TFEB target genes whose expression was upregulated in the *gpr137ba*-mutant pool (Fig. 8j). In summary, this analysis revealed some phenotypic similarities between zebrafish mutants for *gpr137ba* and *rraga*, providing evidence that GPR137B regulates the activity of RagA and, as a consequence, the expression of TFEB targets. Together, the cellular effects of these knockouts indicate that GPR137B also regulates some aspects of Rag function in vivo.

Discussion

Our genome-wide siRNA screen identified GPR137B as a regulator of mTORC1 activation and localization. We focused on GPR137B in part because of its homology to GPCRs, as GPCRs are among the most prominent drug targets in clinical use and because mTORC1 and other lysosomal regulatory pathway components have emerged as promising therapeutic targets for cancer and other diseases[52]. GPR137B has two human homologues that we show also localize to lysosomes and regulate mTORC1 translocation (Fig. 2g and Supplementary Fig. 2f,g). When we performed a sequence homology analysis across multiple eukaryotes[53], we found that genes in the GPR137 family have roots in early eukaryotes, with *GPR137B* homologues being present in *Dictyostelium discoideum*, *Monosiga Bervicollis*, many invertebrates and all vertebrates (Supplementary Fig. 8g). Notably, the mTORC1 regulators Rag, Ragulator and GPR137s all have ancient roots, but Ragulator and GPR137s can each individually or both be lost in different evolutionary branches, suggesting that different species may use alternative control mechanisms to regulate Rags and mTORC1.

Our study shows that knockdown and added expression of GPR137B reduces and increases, respectively, amino acid-triggered mTORC1 translocation to lysosomes and mTORC1 activity. Furthermore, increased expression of GPR137B can activate mTORC1 even under amino acid-starved conditions (Fig. 2f). We provide different lines of evidence that GPR137B regulates mTORC1 through regulation of both the localization and the activity of Rags. First, GPR137B no longer regulates mTORC1 lysosomal localization in RagA/B-knockout cells (Fig. 3b,c). Second, the binding interaction between RagA-GTP and mTORC1 shows that GPR137B regulates the GTP-loading state of RagA (Fig. 5a,b). Third, we show that GPR137B interacts with RagA and increases Rag recruitment to lysosomes (Fig. 4d). We also showed synergistic control of mTORC1 translocation by GPR137B and Rags in amino acid-starved cells, where mTORC1 recruitment increases in parallel with increasing concentrations of both Rags and GPR137B (Fig. 5c–e and Supplementary Fig. 6b) and significant reduction in mTORC1 translocation when DN Rags are co-expressed, suggesting that GPR137B regulates RagA-GTP loading without additional rate-limiting factors.

Our study further revealed that, in response to amino acid stimulation, RagA and RagC dissociate faster from lysosomes along with mTORC1 as a result of RagA-GTP loading (Fig. 6). In support of such a model, we further show that Rags and raptor remain bound to each other while freely diffusing in the cytoplasm (Fig. 7). This is consistent with the interpretation that GPR137B regulates the formation of active Rag–mTORC1 complexes at lysosomes in an activation cycle in which the activated Rag–mTORC1 complexes later dissociate from the lysosomes to potentially activate substrates elsewhere in the cell until Rag is inactivated.

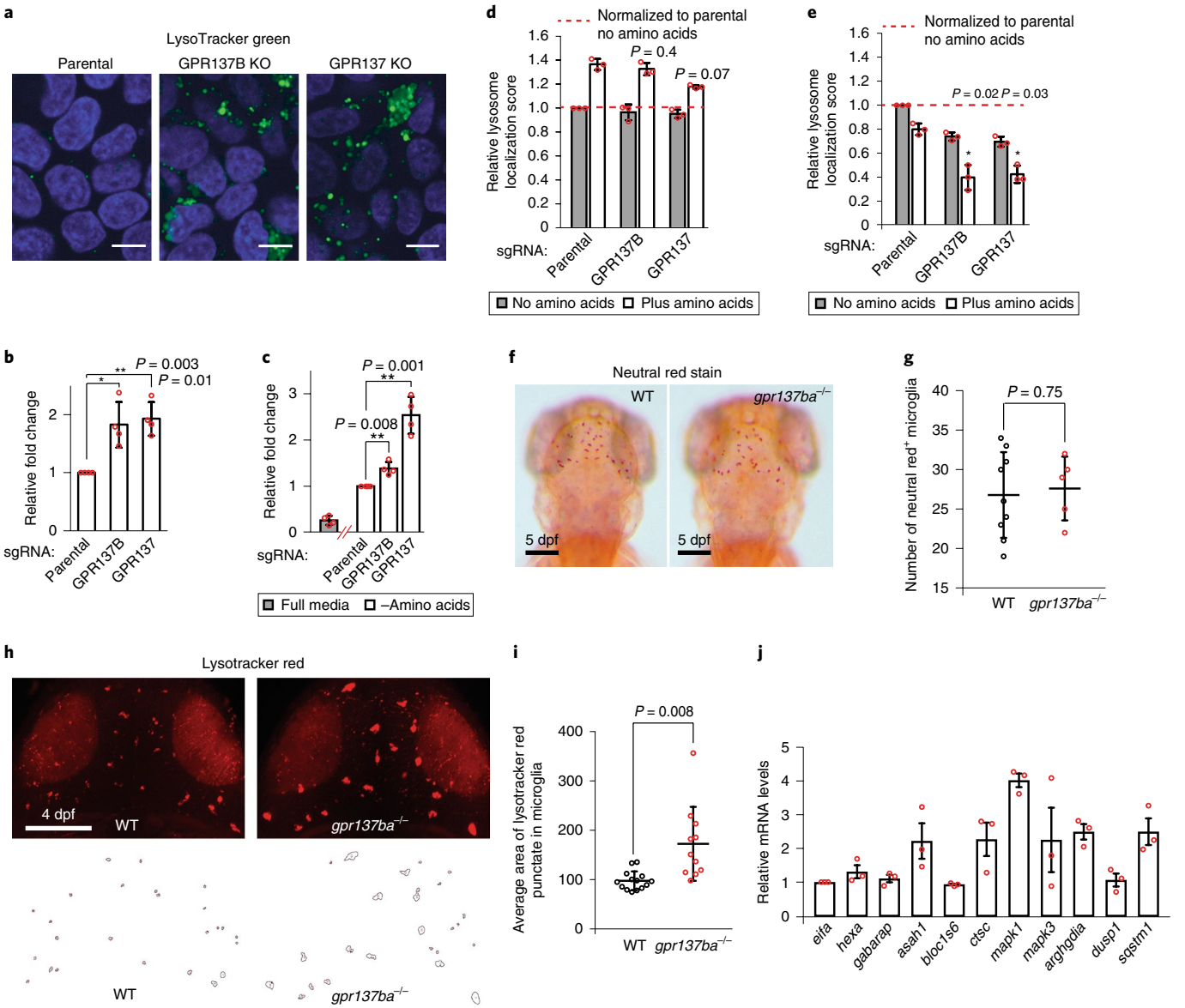


Fig. 8 | Knockout of human *GPR137B* and *gpr137ba* zebrafish mutants show defects similar to Rag pathway mutants. a,**b**, Confocal images of HAP1 parental, GPR137B-knockout (KO) and GPR137-KO cells stained with Hoechst and LysoTracker green (**a**). Quantification is shown in **b**. **c**, HAP1 GPR137-KO and GPR137B-KO cells have an increased number of autophagosomes and/or autolysosomes as measured by endogenous LC3B puncta in response to amino acid starvation. KO clones have significant upregulation from parental cells. In **b** and **c**, data are mean ± s.d.; $n = 4$ independent experiments (ratio paired *t*-test). **d**, Amino acid-induced mTOR translocation is not significantly different in HAP1 GPR137B-KO and GPR137-KO cells. **e**, Lysosomal localization of RagA is reduced in HAP1 GPR137B-KO and GPR137-KO cells. Every KO has significant downregulation from parental cells. $n = 3$ independent experiments in **d** and **e**. Data represent mean ± s.d. (one-way ANOVA analysis followed by Tukey's test). **f**, Wild-type and *gpr137ba*$^{-/-}$ zebrafish have comparable numbers of neutral red-positive microglia. **g**, Quantitative analysis of **f** using an unpaired, parametric, two-tailed *t*-test with Welch's correction. Wild type: $n = 9$ animals; *gpr137ba*$^{-/-}$: $n = 5$ animals. Centre values indicate the mean and the error bars represent s.e.m. **h**, LysoTracker red staining in wild-type and *gpr137ba*$^{-/-}$ zebrafish larvae show enlarged lysosomal compartments in the microglia of *gpr137ba*$^{-/-}$ fish. Scale bar, 50 µm. LysoTracker red-positive compartments are segmented and analysed for area in wild-type and *gpr137ba*$^{-/-}$ zebrafish. **i**, Quantification of the area of LysoTracker red punctae in zebrafish microglia shows that *gpr137ba*$^{-/-}$ larvae ($n = 11$) have significantly larger LysoTracker red-positive compartments relative to wild-type larvae ($n = 14$). Data points represent the average area of the punctae in a single animal. The mean values and s.e.m. are shown (unpaired, parametric, two-tailed *t*-test with Welch's correction). **j**, Quantitative PCR analysis of TFEB targets in pooled *gpr137ba*$^{-/-}$ zebrafish relative to a pool of heterozygous (*gpr137ba*$^{+/-}$) controls ($n = 15$–16 animals in each pool); mutations in *gpr137* and *gpr137c* are randomly assorted in the pools (see the main text and Methods). Targets of TFEB that are significantly upregulated by comparing $^{\Delta\Delta}$CT values include: *arghgdia*: $P = 0.01$, *mapk1*: $P = 0.001$, *sqstm1*: $P = 0.001$ and *ctsc*: $P = 0.05$. The mean values and s.e.m. are shown (unpaired, parametric, two-tailed *t*-test with Welch's correction). $^{*}P < 0.05$, $^{**}P < 0.01$.

We investigated knockouts of GPR137B in human HAP1 cells and in developing zebrafish. Previous studies of RagA/B knockouts in mouse and fish showed that cells can compensate and regulate mTORC1 signalling in a lysosome-independent manner when they lose Rags[22,23,25]. However, knockouts of Rags and Rag regulators[23,25–27] showed a marked increase in accumulation of autophagosomes and/or autolysosomes as well as lysosomal compartment expansion. Similar to Rag-mutant cells, our study showed that

knockout of GPR137B, or of GPR137, caused an increase in the number of LC3B-positive puncta as well as enlarged lysosomal compartments in human cells (Fig. 8a–c). Furthermore, similar to RagA-mutant fish, lysosomes were expanded in the microglia of *gpr137ba* zebrafish mutants (Fig. 8h,i), and targets of the lysosomal transcription factor TFEB, which is repressed by RagA, are upregulated in *gpr137ba*-mutant zebrafish (Fig. 8j). Together, these results suggest that GPR137B knockout has overlapping cellular and physiological effects with knockouts of RagA/B and of two Rag regulators, consistent with the interpretation that GPR137B has a cellular and organismal function to regulate Rags.

Finally, GPR137B is, to our knowledge, unique in that its expression can increase both Rag and mTORC1 localization to lysosomes even in the absence of amino acids, and can regulate a dynamic cycle of RagA activation and lysosome dissociation. Given the key roles of mTORC1 signalling in many cancers, it is interesting that a few reports, without providing molecular mechanisms, have suggested a link between GPR137 and GPR137B and different types of cancers[54–57]. Together with our mechanistic results on the role of GPR137B in Rag and mTORC1 regulation, this suggests that the three human GPCR-like GPR137 genes are potential therapeutic targets for cancers that depend on RagA and/or mTORC1 signalling for growth and survival.

Online content

Any methods, additional references, Nature Research reporting summaries, source data, statements of code and data availability and associated accession codes are available at https://doi.org/10.1038/s41556-019-0321-6.

Received: 1 November 2017; Accepted: 27 March 2019;
Published online: 29 April 2019

References

1. Hirose, E., Nakashima, N., Sekiguchi, T. & Nishimoto, T. RagA is a functional homologue of *S. cerevisiae* Gtr1p involved in the Ran/Gsp1-GTPase pathway. *J. Cell Sci.* **111**, 11–21 (1998).
2. Schürmann, A., Brauers, A., Massmann, S., Becker, W. & Joost, H. G. Cloning of a novel family of mammalian GTP-binding proteins (RagA, RagBs, RagB1) with remote similarity to the Ras-related GTPases. *J. Biol. Chem.* **270**, 28982–28988 (1995).
3. Sekiguchi, T., Hirose, E., Nakashima, N., Ii, M. & Nishimoto, T. Novel G proteins, Rag C and Rag D, interact with GTP-binding proteins, Rag A and Rag B. *J. Biol. Chem.* **276**, 7246–7257 (2001).
4. Sancak, Y. et al. The Rag GTPases bind raptor and mediate amino acid signaling to mTORC1. *Science* **320**, 1496–1501 (2008).
5. Kim, E., Goraksha-Hicks, P., Li, L., Neufeld, T. P. & Guan, K.-L. Regulation of TORC1 by Rag GTPases in nutrient response. *Nat. Cell Biol.* **10**, 935–945 (2008).
6. Sancak, Y. et al. Ragulator–Rag complex targets mTORC1 to the lysosomal surface and is necessary for its activation by amino acids. *Cell* **141**, 290–303 (2010).
7. Bar-Peled, L., Schweitzer, L. D., Zoncu, R. & Sabatini, D. M. Ragulator is a GEF for the Rag GTPases that signal amino acid levels to mTORC1. *Cell* **150**, 1196–1208 (2012).
8. Bar-Peled, L. et al. A tumor suppressor complex with GAP activity for the Rag GTPases that signal amino acid sufficiency to mTORC1. *Science* **340**, 1100–1106 (2013).
9. Panchaud, N., Péli-Gulli, M.-P. & De Virgilio, C. Amino acid deprivation inhibits TORC1 through a GTPase-activating protein complex for the Rag family GTPase Gtr1. *Sci. Signal.* **6**, ra42 (2013).
10. Efeyan, A. et al. Regulation of mTORC1 by the Rag GTPases is necessary for neonatal autophagy and survival. *Nature* **493**, 679–683 (2013).
11. Ricoult, S. J. H. & Manning, B. D. The multifaceted role of mTORC1 in the control of lipid metabolism. *EMBO Rep.* **14**, 242–251 (2012).
12. Settembre, C. et al. TFEB links autophagy to lysosomal biogenesis. *Science* **332**, 1429–1433 (2011).
13. Martina, J. A. & Puertollano, R. Rag GTPases mediate amino acid-dependent recruitment of TFEB and MITF to lysosomes. *J. Cell Biol.* **200**, 475–491 (2013).
14. Huang, J. & Manning, B. D. A complex interplay between Akt, TSC2 and the two mTOR complexes. *Biochem. Soc. Trans.* **37**, 217–222 (2009).
15. Inoki, K., Zhu, T. & Guan, K.-L. TSC2 mediates cellular energy response to control cell growth and survival. *Cell* **115**, 577–590 (2003).
16. Potter, C. J., Pedraza, L. G. & Xu, T. Akt regulates growth by directly phosphorylating Tsc2. *Nat. Cell Biol.* **4**, 658–665 (2002).
17. Linares, J. F. et al. K63 polyubiquitination and activation of mTOR by the p62–TRAF6 complex in nutrient-activated cells. *Mol. Cell* **51**, 283–296 (2013).
18. Zoncu, R. et al. mTORC1 senses lysosomal amino acids through an inside-out mechanism that requires the vacuolar H^+-ATPase. *Science* **334**, 678–683 (2011).
19. Rebsamen, M. et al. SLC38A9 is a component of the lysosomal amino acid sensing machinery that controls mTORC1. *Nature* **519**, 477–481 (2015).
20. Wang, S. et al. Metabolism. Lysosomal amino acid transporter SLC38A9 signals arginine sufficiency to mTORC1. *Science* **347**, 188–194 (2015).
21. Jung, J., Genau, H. M. & Behrends, C. Amino acid-dependent mTORC1 regulation by the lysosomal membrane protein SLC38A9. *Mol. Cell. Biol.* **35**, 2479–2494 (2015).
22. Efeyan, A. et al. RagA, but not RagB, is essential for embryonic development and adult mice. *Dev. Cell* **29**, 321–329 (2014).
23. Kim, Y. C. et al. Rag GTPases are cardioprotective by regulating lysosomal function. *Nat. Commun.* **5**, 4241 (2014).
24. Averous, J. et al. Requirement for lysosomal localization of mTOR for its activation differs between leucine and other amino acids. *Cell. Signal.* **26**, 1918–1927 (2014).
25. Shen, K., Sidik, H. & Talbot, W. S. The Rag–Ragulator complex regulates lysosome function and phagocytic flux in microglia. *Cell Rep.* **14**, 547–559 (2016).
26. Cai, W., Wei, Y., Jarnik, M., Reich, J. & Lilly, M. A. The GATOR2 component Wdr24 regulates TORC1 activity and lysosome function. *PLoS Genet.* **12**, e1006036 (2016).
27. Soma-Nagae, T. et al. The lysosomal signaling anchor p18/LAMTOR1 controls epidermal development by regulating lysosome-mediated catabolic processes. *J. Cell Sci.* **126**, 3575–3584 (2013).
28. Ruvinsky, I. & Meyuhas, O. Ribosomal protein S6 phosphorylation: from protein synthesis to cell size. *Trends Biochem. Sci.* **31**, 342–348 (2006).
29. Rosner, M. & Hengstschläger, M. Evidence for cell cycle-dependent, rapamycin-resistant phosphorylation of ribosomal protein S6 at S240/244. *Amino Acids* **39**, 1487–1492 (2010).
30. Beugnet, A., Tee, A. R., Taylor, P. M. & Proud, C. G. Regulation of targets of mTOR (mammalian target of rapamycin) signalling by intracellular amino acid availability. *Biochem. J.* **372**, 555–566 (2003).
31. Gao, J. et al. TM7SF1 (GPR137B): a novel lysosome integral membrane protein. *Mol. Biol. Rep.* **39**, 8883–8889 (2012).
32. Chan, E. Y. mTORC1 phosphorylates the ULK1–mAtg13–FIP200 autophagy regulatory complex. *Sci. Signal.* **2**, pe51 (2009).
33. Bjørkøy, G. et al. p62/SQSTM1 forms protein aggregates degraded by autophagy and has a protective effect on huntingtin-induced cell death. *J. Cell Biol.* **171**, 603–614 (2005).
34. Gingras, A.-C., Raught, B. & Sonenberg, N. Regulation of translation initiation by FRAP/mTOR. *Genes Dev.* **15**, 807–826 (2001).
35. Miron, M., Lasko, P. & Sonenberg, N. Signaling from Akt to FRAP/TOR targets both 4E-BP and S6K in *Drosophila melanogaster*. *Mol. Cell. Biol.* **23**, 9117–9126 (2003).
36. Fingar, D. C., Salama, S., Tsou, C., Harlow, E. & Blenis, J. Mammalian cell size is controlled by mTOR and its downstream targets S6K1 and 4EBP1/eIF4E. *Genes Dev.* **16**, 1472–1487 (2002).
37. Wolfson, R. L. et al. Sestrin2 is a leucine sensor for the mTORC1 pathway. *Science* **351**, 43–48 (2016).
38. Chantranupong, L. et al. The sestrins interact with GATOR2 to negatively regulate the amino-acid-sensing pathway upstream of mTORC1. *Cell Rep.* **9**, 1–8 (2014).
39. Kim, J. S. et al. Sestrin2 inhibits mTORC1 through modulation of GATOR complexes. *Sci. Rep.* **5**, 9502 (2015).
40. Parmigiani, A. et al. Sestrins inhibit mTORC1 kinase activation through the GATOR complex. *Cell Rep.* **9**, 1281–1291 (2014).
41. Peng, M., Yin, N. & Li, M. O. Sestrins function as guanine nucleotide dissociation inhibitors for Rag GTPases to control mTORC1 signaling. *Cell* **159**, 122–133 (2014).
42. Oshiro, N., Rapley, J. & Avruch, J. Amino acids activate mammalian target of rapamycin (mTOR) complex 1 without changing Rag GTPase guanyl nucleotide charging. *J. Biol. Chem.* **289**, 2658–2674 (2014).
43. Deng, L. et al. The ubiquitination of rag A GTPase by RNF152 negatively regulates mTORC1 activation. *Mol. Cell* **58**, 804–818 (2015).
44. Jin, G. et al. Skp2-mediated RagA ubiquitination elicits a negative feedback to prevent amino-acid-dependent mTORC1 hyperactivation by recruiting GATOR1. *Mol. Cell* **58**, 989–1000 (2015).
45. Lawrence, R. E. et al. A nutrient-induced affinity switch controls mTORC1 activation by its Rag GTPase–Ragulator lysosomal scaffold. *Nat. Cell Biol.* **20**, 1052–1063 (2018).

46. Zhou, X. et al. Dynamic visualization of mTORC1 activity in living cells. *Cell Rep.* **10**, 1767–1777 (2015).
47. Manifava, M. et al. Dynamics of mTORC1 activation in response to amino acids. *eLife* **5**, e19960 (2016).
48. Shen, K., Teruel, M. N., Subramanian, K. & Meyer, T. CaMKIIβ functions as an F-actin targeting module that localizes CaMKIIα/β heterooligomers to dendritic spines. *Neuron* **21**, 593–606 (1998).
49. Gong, R. et al. Crystal structure of the Gtr1p–Gtr2p complex reveals new insights into the amino acid-induced TORC1 activation. *Genes Dev.* **25**, 1668–1673 (2011).
50. Napolitano, G. & Ballabio, A. TFEB at a glance. *J. Cell Sci.* **129**, 2475–2481 (2016).
51. Meireles, A. M. et al. The lysosomal transcription factor TFEB represses myelination downstream of the Rag–Ragulator complex. *Dev. Cell* **47**, 319–330.e5 (2018).
52. Xie, J., Wang, X. & Proud, C. G. mTOR inhibitors in cancer therapy. *F1000Res.* **5**, 2078 (2016).
53. Dey, G., Jaimovich, A., Collins, S. R., Seki, A. & Meyer, T. Systematic discovery of human gene function and principles of modular organization through phylogenetic profiling. *Cell Rep.* **10**, 993–1006 (2015).
54. Wang, C., Liang, Q., Chen, G., Jing, J. & Wang, S. Inhibition of *GPR137* suppresses proliferation of medulloblastoma cells in vitro. *Biotechnol. Appl. Biochem.* **62**, 868–873 (2015).
55. Cui, X. et al. Knockdown of *GPR137* by RNAi inhibits pancreatic cancer cell growth and induces apoptosis. *Biotechnol. Appl. Biochem.* **62**, 861–867 (2015).
56. Andrade, V. P. et al. Gene expression profiling of lobular carcinoma in situ reveals candidate precursor genes for invasion. *Mol. Oncol.* **9**, 772–782 (2015).
57. Brunetti, M. et al. Recurrent fusion transcripts in squamous cell carcinomas of the vulva. *Oncotarget* **8**, 16843–16850 (2017).

Acknowledgements

K.S. and H.I. were supported by fellowships from A*STAR Singapore and AHA (18POST33990334), respectively. W.S.T. is a Catherine R. Kennedy and Daniel L. Grossman Fellow in Human Biology. Work in the Talbot lab was supported by the NIH grant R01NS050223 and the NMSS grant RG-1707–28694, and in the Meyer lab by R35 GM127026 and UL1TR001085 and the Stanford SPARK Translational Program. We thank D. Garbett, M. Chung, S. Cappell, S. Spencer, S. Collins, M. Koberlin and other lab members for discussions and critical reading of the manuscript, A. Bisaria for plasmids, M. Lopez for the NPC1 construct and D. Solow-Cordero at the HTBC for help in preparing siRNAs for screening.

Author contributions

K.S. generated the TALEN mutations in zebrafish and analysed microglia. H.I. generated the CRISPR mutations in zebrafish and performed quantitative PCR. K.S., H.I. and W.S.T. designed the zebrafish experiments, analysed the data and contributed to writing the manuscript. L.G. and T.M. planned the initial siRNA screen and follow-up experiments characterizing GPR137B function. T.M. supervised the project and wrote most of the manuscript together with L.G. L.G. and T.M. planned and L.G. performed and analysed all cell-based experiments. A.S., L.G. and T.M. planned and A.S. performed and analysed all biochemistry studies of GPR137B. K.H. and L.G. performed the initial siRNA screen and R.W. helped with the initial analysis of the screen. A.H. helped with imaging. G.D. helped with image analysis and evolutionary analysis of GPR137B. X.G. and J.L. helped with some cell biology and biochemical studies.

Competing interests

The authors declare no competing interests.

Additional information

Supplementary information is available for this paper at https://doi.org/10.1038/s41556-019-0321-6.

Reprints and permissions information is available at www.nature.com/reprints.

Correspondence and requests for materials should be addressed to T.M.

Publisher's note: Springer Nature remains neutral with regard to jurisdictional claims in published maps and institutional affiliations.

© The Author(s), under exclusive licence to Springer Nature Limited 2019

Methods

Cell lines. HS68 primary fibroblast, HeLa and HEK293T cells were obtained from the American Type Culture Collection (ATCC). CRISPR–Cas9-edited HAP1 cells were purchased from Horizon Discovery. RagA/B-knockout and parental MEFs were kindly provided by K.-L. Guan's lab (UC San Diego). *NRPL3* sgRNA (sgNPRL3) and parental HEK293E cells, sgSestrin1/2/3 and parental HEK293T cells were kindly provided by D. Sabatini's lab (Massachusetts Institute of Technology, Boston).

Immunofluorescence. Cells were fixed in 4% formaldehyde in PBS for 30 min at room temperature, washed with PBS followed by 15 min of 0.2% Triton X-100 permeabilization on ice. BSA (3%) in 1× PBS was used for blocking for 30 min at room temperature. Primary antibodies were added overnight at 4 °C (Hoechst and fluorescent secondary antibodies were added after washing for 1–2 h at room temperature). Images were taken either with a ×20 air objective on an automated inverted epifluorescence microscope (ImageXpressMicro, Molecular Devices) or with a ×40 or ×100 oil objective on a confocal microscope (Leica TCS SP2 AOBS or 3i imaging system). See the section 'Fixed/live-cell imaging' for a more detailed description; see Supplementary Table 5 for antibody information.

Zebrafish lines and maintenance. The Tupfel long-fin (TL) strain of *Danio rerio* was used for all zebrafish experiments. All work with zebrafish was conducted with approval from the Stanford University Institutional Animal Care and Use Committee. Embryos and larvae were treated with 0.003% 1-phenyl-2-thiourea (PTU) to inhibit pigmentation and anaesthetized with 0.016% (w/v) tricaine prior to experimental procedures.

Genome-wide siRNA screen and hit selection. The primary screen was performed using human primary foreskin fibroblasts (Hs68 cells). Serum was removed to maximize the amino acid-induced signal. Cells were stimulated after amino acid removal with a 1× mixture of all amino acids without glutamine (Fig. 1b, schematic). An siARRAY whole human genome siRNA library from Thermo Fisher Scientific (formerly Dharmacon; G-005000–025), containing 21,041 siRNA pools in 267 × 96-well plates, 80 siRNA pools per plate, was screened using a 384-well formatted assay. Three replicates of each mother siRNA plate were tested at 10 nM concentration in the primary screen; a total of 204 384-well plates. All transfections were done using a Vprep (Velocity 11) with a 96-tip disposable tip head. Lipofectamine 2000 addition and cell addition were done with a Wellmate Dispenser (Matrix). All washing steps, including serum starvation and amino acid starvation were done using the Plate Washer (Bio-TEK). Hs68 cells were reverse transfected and the transfection mix was removed 18–24 h later. Cells were then serum starved with DMEM/0.1% BSA to keep cell numbers consistent among wells. Post-transfection (68–72 h), cells were amino acid starved in 1.5% BSA/DPBS for 3 h and restimulated with an amino acid mixture (1× amino acid) prepared from diluting 50× essential amino acids and 100× non-essential amino acids in 1.5% BSA/DPBS. Cells were fixed and stained with an antibody against rpS6 phosphorylated at 240/244. Phosphorylation of rpS6 was imaged with an automated microscope (Axon, Molecular Devices), and integrated fluorescence intensity was quantified using CellProfiler[58].

Primary screen analysis. Using automated fluorescence imaging and automated analysis of antibody staining, we averaged the integrated single-cell rpS6 phosphorylation intensities across all cells in a single well. The mean rpS6 phosphorylation intensity for each well was calculated as the deviation from the median of the surrounding 20 wells in the 384-well plate, to minimize regional plate artefacts. The standard deviations (s.d.) of the three replicates of each siRNA treatment (each plate was assayed in parallel in triplicate) were used as a measure of experimental variability[59,60]. The region-corrected means were normalized to the average of the triplicate s.d. for the entire plate to generate a Z-score = $(X-\mu)/\sigma$. The parameter μ was estimated using the regional median and the σ parameters were estimated using replicates in each triplicate set. A comparison to nearby 20 wells was used as the library is not randomly organized. Z-scores were normalized to the median Z-score of positive controls (*RHEB* siRNA (siRHEB) or siTSC2 controls) in each triplicate set. The resulting fold-change values were used to create a rank-ordered list of genes and the top 750 genes were selected as hits. An additional list of hits (with a minimum Z-score of 2) was selected based on an additional criterion of matching functional identifiers or literature data (for example, kinase and exchange factor). With these added hits, a total of 1,231 genes were selected for further analysis.

Deconvolution of siRNA pools. Using the same assay as in the primary screen, each single siRNA of the 1,231 selected pools was tested separately again in a 384-well formatted assay (4 siRNAs targeting the same gene in each pool). Each siRNA was transfected at 10 nM concentration. A quadrant of each plate was filled with siRNA targeting a scrambled sequence (negative controls). The mean integrated phospho-rpS6 intensity for each well was region corrected by subtracting the average of the mean phospho-rpS6 intensities of the negative controls in a 22-well neighbourhood, and then divided by the s.d. of the mean phospho-rpS6 intensities of all of the negative control wells on the same plate. The generated Z-scores were then averaged across duplicates. For each of the original 1,231 pools, the deconvolution score was calculated as the average of the second and third strongest single siRNAs. We averaged the second and third strongest siRNA as we noticed a tight correlation between the first siRNA and the primary screen pool value (Supplementary Fig. 1c, left), which argued that the strongest siRNA largely recapitulates the screen phenotype. This also means that the averaged second and third hit can provide a second independent test for off-target effects (Supplementary Fig. 1c, right). The resulting rank-ordered list of deconvolution scores was at the end manually pruned (removing high-scoring genes with functions probably unrelated or indirectly related to mTOR signalling, such as secreted or extracellular proteins, and adding a few lower-scoring genes with relevant functional characteristics) to generate a total of 427 deconvolution hits that we further investigated.

mTOR translocation screen. The 427 hits were then assayed for their effect on mTOR translocation. The single siRNA with the strongest phospho-rpS6 phenotype for each hit (see 'Deconvolution of siRNA pools' above) was tested in duplicate in 96-well format at a concentration of 5 nM and assayed in parallel on a single plate for phospho-rpS6. Cells were reverse transfected using the same conditions as the primary screen, except both the transfection and the assay were performed manually using multichannel pipettes. Cells were starved of amino acids for 4 h in 1.5% BSA/DPBS and restimulated with cycloheximide for 5 min (mTOR translocation) or 30 min (rpS6 phosphorylation). The plates were fixed and stained with antibodies against mTOR and Lamp2 or phospho-rpS6 (240/244). The correlation coefficient between the intensity of segmented puncta in the mTOR and Lamp2 channels was calculated for each well and averaged across duplicates. A Z-score for mTOR translocation was generated by subtracting the plate median and normalizing the result by the plate s.d. A Z-score for the parallel phospho-rpS6 experiment was generated by subtracting the mean of the negative control wells (scrambled siRNA) and normalizing the result to their s.d. The plate median was not used in this case because all of the genes were expected to perturb phospho-rpS6 levels to some extent, having been selected as deconvolution hits in the first place. Hits with a translocation Z-score below −1.8 and rpS6 phosphorylation below −1.6 were considered for further analysis.

Bioinformatics. Ingenuity Systems pathway analysis (www.ingenuity.com) was used to identify enriched pathways and draw networks. The subset of hits solely chosen based on rank selection were uploaded into Ingenuity pathway analysis and the most enriched canonical pathways or diseases were identified. Fisher's exact test was used to calculate a *P* value.

Cell culture and reagents. Hs68 primary fibroblasts, HeLa cells, MEFs and HEK293T cells were cultured in 10% FBS/DMEM/PSG (Gibco) medium. HAP1 parental and knockout cells generated by CRISPR–Cas9 were purchased from Horizon Discovery and cultured in 10% FBS/IMDM. Lipofectamine 2000, DPBS media used for starvation, 50× essential amino acids and 100× non-essential amino acids were obtained from Life Technologies. BSA, cycloheximide and PMA were from Sigma-Aldrich. Triton X-100 was from Sigma, and 16% formaldehyde was from Ted Pella. *n*-Octyl-β-D-glucopyranoside was from Affymetrix. GeneSilencer (Genlantis) was used for siRNA and plasmid co-transfection in HeLa cells. Fugene 6 and X-tremeGENE HP (Roche Applied Science) were used for plasmid transfection into HeLa and HEK293T cells. Lipofectamine 2000 was used to transfect DNA or siRNA into Hs68 and HEK293T cells. The MEF2 Nucleofector Kit was purchased from Lonza to electroporate MEFs using the Amaxa Nucleofector. Rapamycin was purchased from Calbiochem. Torin was purchased from Tocris. Amino acid starvation medium (DMEM without amino acids) was purchased from Athena Enzyme Systems as a custom media. DMEM culture media were used as amino acid addback medium. Amino acid starvation experiments in screen and fluorescence recovery after photobleaching (FRAP) experiments were conducted in 1.5% BSA/DPBS and restimulated with an amino acid mixture (1× AA) added to the starvation media. DMEM without amino acids and 10% dialysed FBS was used as starvation media for all other experiments.

GPR137B reagents and various mTORC1 reagents. siRNAs against *GPR137B* were purchased from Dharmacon as four separate duplexes. The sequence with the strongest effect was GGACUAAAGUAUUCCACAA (3′ untranslated region (UTR)); the second strongest was GCAAUAAUGUAGACUGAUA (3′ UTR). siRNAs against *LAMTOR2* and *LAMTOR3* were purchased from Dharmacon as siGenome Smartpools. cDNAs encoding GPR137 (NM_001170880) and GPR137C (NM_001099652) were purchased from Open Biosystems, now part of GE Healthcare. *GPR137B* cDNA was obtained from in-house human ORFeome collection. All GPR137, GPR137B and GPR137C fluorescently tagged proteins were cloned by recombining the cDNA into Gateway destination vectors. Wild-type Venus-RagC, RagC-Turquoise and Venus-RagA were generated by cloning human ORFeome cDNA into the Gateway destination vector. The LC3-GFP (plasmid no. 24920), rat Lamp1-mRFP-2×FLAG (plasmid no. 34611) and YPF-raptor (plasmid no. 73385) were obtained from Addgene. Lamp1-Turquoise was subcloned from rat Lamp1-mRFP-2×FLAG using Gateway destination vectors. pRK5-haemagglutinin (HA) glutathione *S*-transferase (GST) RagA 66L (Addgene

plasmid no. 19300) and pRK5-HA GST RagA 21L (Addgene plasmid no. 19299) were gifts from D. Sabatini. YFP-RagC T75N, cyan fluorescent protein (CFP)-RagC Q120L and CFP-RagA T21N were gifts from W. D. Heo. NPC1-YFP-2×FLAG was a gift from M. Lopez. GPR137B-3×FLAG and rat Lamp1-3×FLAG were subcloned into pPBbsr2-IRES-blasticidin, and GPR137B-HA was subcloned into the pLV-EF1a-IRES puromycin vector using Gibson assembly (New England Biolabs). C1-mRuby-RagC was generated from Gibson assembly using C1-YFP and mRuby-T-Plastin and subcloned into a Gateway destination vector with wild-type RagC. Infrared fluorescent protein (iRFP)-CAAX was generated by PCR of iRFP with primers encoding the CAAX sequence and entry into pLenti-IRES-Puro and also the Clonetech C1 vector. HEK293T cells stably expressing GPR137B-3×FLAG and Lamp1-3×FLAG were generated using the PiggyBac transposon system (System Biosciences). A GPR137B-HA stable cell line was generated by lentivirus infection. Positive clones were selected using indicated antibiotics.

Fixed/live-cell imaging. High-resolution images (Figs. 1d and 2b,c,e) were acquired on a scanning confocal system (Leica SP2-AOBS) using a ×40 1.25 NA oil immersion objective. Lower-resolution images (Figs. 2g,l, 3a,b,d and 6b,e and Supplementary Figs. 2f and 3a) were acquired on a fully automated fluorescence microscope (ImageXpress Micro XL, Molecular Devices) with a Sola Light Engine (Lumencor), a Zyla 5.5 sCMOS camera (Andor) and using a ×20 0.45 NA Plan Fluor objective (Nikon) with no binning. A ×4 0.13 (NA) objective with no binning was used for Fig. 1b. FRAP images, plasma membrane translocation images and LysoTracker green images (Figs. 6g, 7a,b and 8a and Supplementary Fig. 7a,b) were acquired on an automated widefield/Yokogawa spinning-disc confocal fluorescence microscope system (Intelligent Imaging Innovations, 3i), using either a Nikon ×40 1.3 NA oil objective or a ×100 1.4 NA oil objective, a 3i laser stack (405, 442, 488, 514, 561 and 640 nm), a 3i 'Vector' photomanipulation device, an epifluorescence light source (Sutter Lambda XL), a Yokogawa CSU-W1 scanning head with dual camera port and two sCMOS cameras (Andor Zyla 4.2). These experiments were performed inside an environmental chamber (Haison). FRAP experiments (Fig. 6g–l) were either carried out using a ×40 oil objective at 2×2 binning with an epifluorescence light source or a ×100 oil objective at 2×2 binning (Supplementary Fig. 6e). A 515-nm laser was used for photobleaching and images were acquired at 10 s per frame in CFP and YFP EPI channels after photobleaching. Plasma membrane translocation images (Fig. 7a,b and Supplementary Fig. 7a,b) were acquired in confocal mode using a ×100 oil objective at 2×2 binning and 514-nm, 561-nm and 640-nm lasers. LysoTracker green images (Fig. 8a) were acquired using a ×40 oil objective and 405-nm and 488-nm lasers.

Analysis of lysosomal localization of mTOR. Fluorescence imaging of mTOR translocation was based on immunostaining using anti-mTOR and anti-Lamp2 antibodies. For screening analysis of the 427 genes, a custom-written MATLAB script was used to cross-correlate the mTOR and Lamp2 signals in a perinuclear region as a measure for relative colocalization (Figs. 1e and 2d). A more quantitative mTOR localization and translocation parameter (a slower but more automated analysis) was developed for the remainder of the figures (See Supplementary Code 1). In this analysis, we identified local Lamp2-positive vesicles and created a binary lysosome mask. We used this mask to subtract a local background for the analysis of mTOR localization and translocation. More specifically, the analysis started by first segmenting nuclei and calculating a distance matrix of the closest cytoplasmic pixels to the nucleus. We used a ring identified by >8 pixels and <20 pixels away from the nucleus as the perinuclear region where we identified Lamp2-positive vesicles and measured mTOR intensity at these Lamp2-positive sites. The binary mask of Lamp2 puncta was identified by finding the peak intensity values after subtracting the non-lysosomal background. This Lamp2 puncta segmentation was then used to measure the relative intensity of pixels in the mTOR channel above background. As the lysosomal regions are a small fraction of the area, we used a shifted mask (several pixels shifted in different directions) to measure and subtract a randomized background to detect a lysosomal mTOR intensity over the averaged background value. The mTOR pixel values in the Lamp2 puncta per cell were averaged to derive a 'relative translocation score' for that cell (Fig. 2f, Supplementary Fig. 2b,c and the remainder of the figures). To quantify the levels of RagA, RagC and Lamp1 at the lysosome (Fig. 6a–f), we substituted RagA, RagC and Lamp1 for mTOR staining and used an identical automated analysis. For each experiment, 12–25 sites per 96 well were imaged, and at least 1,000 cells were analysed per well and 2–4 wells were included per independent experiment. Statistical analysis was performed either by comparing the averages of control versus treated wells over independent experiments (Figs. 2f,h,j, 3c–e, 4e,f, 6a,d,k,m, 7c and 8b–e,i,j and Supplementary Figs. 1e, 2a–d,h,j, 4e,g and 6e, f) or comparing the averages of transfected cells versus that of non-transfected cells in the same well (Figs. 2k and 4d and Supplementary Figs. 2h,i and 4f,h). Parametric, two-tailed Student's *t*-test and one-way analysis of variance (ANOVA) followed by Tukey's test were used as indicated in the figure legends.

Synergy heatmap analysis of Rag and GPR137B. For Fig. 5c, HeLa cells were amino acid starved for 10–12 h, and cells co-expressing Lamp1-Turquoise and Venus-RagC ($n=14{,}004$) or GPR137B-Turquoise and Venus-RagC ($n=14{,}207$) were binned into 10 equal bins of Turquoise intensities and Venus intensities. The average mTOR translocation score for each bin is plotted as a blue-yellow heatmap scaled from 50 to 450. Grey indicates bins where there was an insufficient number of cells. For Fig. 5e, *Rraga/b*$^{-/-}$ MEFs transiently co-expressing either Lamp1-Venus with wild-type HA-RagA/Turquoise-RagC ($n=40{,}061$) or DN HA-RagA/CFP-RagC (T21L/Q120L) ($n=32{,}958$), or GPR137B-Venus with wild-type HA-RagA/Turquoise-RagC ($n=37{,}520$) or DN RagA/CFP-RagC ($n=38{,}902$). We first corrected for fluorophore differences between Turquoise and CFP before generating the heatmaps. We correlated RagA protein levels to RagC fluorescence intensities in the same cell and then normalized DN RagC intensity values by the ratio of the correlation slopes to adjust them to reflect the same amount of RagA proteins at the same wild-type RagC intensities. We plotted all of the single-cell measurements for Rag intensity, Lamp1 or GPR137B intensity and mTOR translocation score and selected a range that represented most values in the histograms. RagC and Lamp1 or GPR137B fluorescence intensities were binned into 10 equal bins, and the average mTOR translocation score of each bin is plotted as a blue-yellow heatmap scaled from 0 to 200. Identical correction and analysis were used for a repeat of this experiment in Supplementary Fig. 6b. $n=31{,}157$ for Lamp1 and wild-type RagA/C, and $n=201{,}168$ for GPR137B and wild-type RagA/C in Supplementary Fig. 6b.

FRAP experiments and analysis. All photobleaching experiments were conducted on the 3i imaging system using a ×40 or ×100 objective (Supplementary Fig. 6e,f). Images were acquired every 10 s and bleaching was set to the sixth frame. Bleaching was set in 515 nm for 1 s one time in a rectangular area. For fluorescence recovery measurements, selected lysosomes were tracked manually in ImageJ using Lamp1-Turquoise or GPR137B-Turquoise as a lysosome mask and the corresponding average RagC intensity was recorded for each frame. A background region containing no cells was first subtracted from the raw intensities and then divided by a neighbouring non-bleached region. All values were then normalized to the frame immediately before bleaching (fifth frame). For bar graphs in Fig. 6k,m, we derived a single measurement by subtracting the fluorescence intensity at frame ten from frame five to represent the relative recovery for each recovery curve, and then averaging the relative recovery for all curves.

Transfection and starvation of HEK293T cells for co-immunoprecipitation. One day prior to DNA transfection, cells were plated on collagen-coated dishes. The next day, GPR137B was transfected using Lipofectamine 2000 (Thermo Fisher Scientific) in Opti-MEM1 (Thermo Fisher Scientific) overnight. Media were changed to 10% FBS containing DMEM (Thermo Fisher Scientific). Cells were harvested 48 h after transfection. For all co-immunoprecipitation experiments, cells were starved and added back for amino acids in DMEM supplemented with dialysed FBS. When phosphorylation of S6K was examined (Fig. 2m), DMEM without FBS was used.

Cell lysis and immunoprecipitation. For amino acid-regulated binding, cells were amino acid starved for 2 h and then amino acids were added back for 10–15 min. Cells were incubated with 1 mg ml^{-1} Dithiobis (succinimidyl propionate) (DSP) for 20 min at room temperature and then the reaction was quenched by treating cells with 100 mM Tris, pH 8.5, for 10 min. Cells were lysed in octyl-glucoside lysis buffer (60 mM *n*-octyl-β-D-glucopyranoside, 50 mM HEPES (pH 7.4), 150 mM NaCl and protease inhibitor cocktail (Thermo Fisher Scientific) and then homogenized with a 25-G needle and centrifuged at 1,100*g* at 4 °C for 5 min to remove nuclei. SDS (0.1%) was added to the supernatant. The lysate was sonicated briefly and then incubated at 4 °C for 1 h followed by centrifugation at 20,000*g* for 60 min. The lysates were adjusted to a total protein concentration of 0.1–0.2 mg ml^{-1} and incubated with the FLAG-M2 affinity gel (catalogue no. 8823, Sigma) or mouse anti-HA (catalogue no. 88837, lot no. QJ224632, Pierce) at 4 °C overnight. The beads were washed three times with ice-cold lysis buffer with 300 mM NaCl and then washed twice with lysis buffer. Immunoprecipitated proteins were denatured in urea-containing SDS sample buffer (final concentration of 62.5 mM Tris-HCl, 12.5% glycerol, 0.01% bromophenol, 300 mM dithiothreitol, 4 M urea and 3% SDS) at 37 °C for 30 min with rotation. The samples were loaded on 4–12% NuPAGE Bis-Tris, 3–8% Tris-acetate precast gels or Bolt 4–12% Bis-Tris plus gels (Life technologies). The signal intensities were analysed by ImageJ (NIH) and graphed using Prism (GraphPad).

GPR137B-FLAG and GPR137B-HA co-immunoprecipitation. To observe amino acid-sensitive GPR137B–GPR137B self-interaction, GPR137B-FLAG and GPR137B-HA were stably co-expressed in *Rraga/b*$^{-/-}$ MEFs or control MEFs at low levels. To achieve this, the upstream open reading frames of pPBbsr2-GPR137b-FLAG and pLV-EF1a-GPR137B-HA were attenuated by adding a TTT sequence[61]. Only earlier passages of cells were used.

MEFs were amino acid starved for 3–4 h, restimulated for 20 min and then DSP crosslinked. The GPR137B complex was immunoprecipitated using a FLAG-M2 affinity gel at 4 °C overnight. The complex was analysed by western blot.

TALEN and CRISPR targeting to generate mutations in zebrafish *gpr137b* homologues. The TAL Effector-Nucleotide Targeter 2.0 (refs. [62,63]) webtool

was used to design a pair of TALENs to target *gpr137c*, *gpr137* and *gpr137ba*. The Golden Gate cloning protocol for creating the TALEN plasmids was used[64]. Plasmids were then transcribed using the Sp6 mMessage mMachine Kit by Ambion. mRNA (400 ng) were injected into one-cell-stage wild-type TL embryos, which were raised to adulthood. To identify founders carrying a null mutation in the germline, we crossed injected fish to the wild type (TL strain) and genotyped a subset of the progeny at 2–3 d post-fertilization (dpf). The TALEN lesions were given the following names and genotyped using the following primers and restriction assays: *gpr137c*, *st117*, 10-bp deletion, forward primer: ttggataagtcggcgtgatag, reverse primer: cgtcctcagagcagaccag, restriction assay using DpnII; *gpr137*, *st118*, 8-bp deletion, forward primer: ccatgagcgtcatttttcctg, reverse primer: acacccgaatgcatcacac, restriction assay using HpaI; *gpr137ba*, *st119*, 20-bp deletion, forward primer: gagcagtgggaagcagaaac, reverse primer: ggtaacgcaaaaccaaccac, restriction assay using SfaNI. All restriction enzymes cleave the wild-type allele, but not the mutant allele. Based on the disruption of the restriction site, we identified founders and raised the remaining F1 progeny to adulthood. F1 heterozygous adults for the respective deletions were crossed to the TL strain to establish a stock.

For CRISPR experiments, sgRNAs were designed using CHOPCHOP. The sgRNA was transcribed from the DNA template with T7 polymerase (E2040S, New England Biolabs) and purified using the mirVana miRNA isolation kit (AM1560, Ambion). Cas9 protein (Macrolab, Berkeley) and ~300 ng sgRNA were injected into one-cell-stage embryos, and embryos were genotyped to detect lesions. The sgRNA used for *gpr137bb* was GGGTCACTACCGGTTGTACC. The efficacy of the sgRNA was determined by sequencing eight individual embryos after PCR using forward primer: GCTATTCCCAGCCACGTGTTC and reverse primer: CACAGGAGATACAGCTCAGTGC.

LysoTracker red and neutral red staining of live zebrafish larvae. Larvae (not selected for gender) at 4 dpf were incubated in a 1:100 dilution of LysoTracker red DND-99 (Invitrogen) in embryo water at 28.5 °C for 45 min, washed twice with embryo water, mounted in 1.5% LMP agarose and imaged with a Zeiss confocal microscope. For the neutral red assay, larvae at 5 dpf (not selected for gender) were incubated in 2.5 μg ml^{-1} neutral red at 28.5 °C for 2.5 h, washed twice with embryo water, mounted in 1.5% LMP agarose and analysed using a dissecting microscope.

Particle analysis in ImageJ. LysoTracker red-stained images were thresholded to generate a binary image and despeckled. 'Analyze particles' with a setting of area of >30 pixels was used to generate overlays and measure the area of LysoTracker red-stained punctae.

Quantitative real-time PCR. Zebrafish larvae were obtained from a cross between *gpr137c*$^{+/-}$; *gpr137*$^{+/-}$; *gpr137ba*$^{-/-}$ male × *gpr137c*$^{-/-}$; *gpr137*$^{+/-}$; *gpr137ba*$^{+/-}$ female adults. At 5 dpf, larvae (not selected for gender) were anaesthetized with tricaine. DNA was prepared from tail fins of individual fish, and the remaining portion of each fish was snap frozen on dry ice. The genotypes of each animal were determined by a PCR assay for the *gpr137ba* lesion and the frozen larvae were pooled based on the genotype for *gpr137ba*. Three batches of 15–16 embryos that were either heterozygous (*gpr137ba*$^{+/-}$) or homozygous (*gpr137ba*$^{-/-}$) mutants were pooled separately to obtain biological triplicates. Total RNA was extracted from pooled embryos using the RNAeasy Kit (Qiagen). cDNA was synthesized using iScript Supermix (1708840, Bio-Rad). Quantitative PCR was performed with SsoAdvancedTM Universal SYBR Green Supermix (1725271, Bio-Rad) on the Bio-Rad CFX384 Real-Time PCR Detection System. All experiments were done in biological and technical triplicates. Transcript levels were normalized to *eif1a*[25,65]. Relative mRNA levels were calculated using $^{\Delta\Delta}$CT.

Statistics and reproducibility. Unpaired, parametric, two-tailed Student's *t*-tests were performed using Prism (GraphPad) to analyse the statistical significance of experiments in Figs. 2f,h,k, 3d, 4e,f, 6m and 7c and Supplementary Figs. 1e, 2c,e,h–j and 6f. Paired, parametric, two-tailed Student's *t*-tests were used for experiments in Fig. 6d,k and Supplementary Figs. 2e,g and 4h, and ratio paired *t*-tests were applied to Figs. 2j, 6a and 8b,c and Supplementary Fig. 2d,i. For multiple group comparisons, one-way ANOVA was performed using GraphPad for Fig. 3c and Supplementary Fig. 2b, and repeated-measures ANOVA was used for Figs. 4d and 8d,e and Supplementary Fig. 4f. All ANOVA analyses were followed by Tukey's test. Unpaired, parametric, two-tailed *t*-test with Welch's correction was used for the fish experiments in Fig. 8g,i,j. A description of each statistical test and *P* values are included with each experimental source data (Supplementary Table 4). Experiments in Figs. 2l,m, 3e, 4a–c and 5e and Supplementary Figs. 1a, 3b, 4a,b,d, 5a and 7a were performed two times independently showing similar results. The experiment in Supplementary Fig. 7b was done once. All other experiments were performed three or more times independently showing similar results.

Reporting Summary. Further information on research design is available in the Nature Research Reporting Summary linked to this article.

Data availability

The screen data that support the findings of this study have been deposited in the PubChem BioAssay under the accession code AID 29260. Statistical source data for Figs. 2–8 and Supplementary Figs. 1, 2, 4–6 and 8 are provided in Supplementary Table 4. All data supporting the findings of this study are available from the corresponding author on request.

Code availability

The MATLAB script for the analysis of lysosomal localization is shared in Supplementary Note.

References

58. Carpenter, A. E. et al. CellProfiler: image analysis software for identifying and quantifying cell phenotypes. *Genome Biol.* **7**, R100 (2006).
59. Paulsen, R. D. et al. A genome-wide siRNA screen reveals diverse cellular processes and pathways that mediate genome stability. *Mol. Cell* **35**, 228–239 (2009).
60. Galvez, T. et al. siRNA screen of the human signaling proteome identifies the PtdIns(3,4,5)P3–mTOR signaling pathway as a primary regulator of transferrin uptake. *Genome Biol.* **8**, R142 (2007).
61. Ferreira, J. P., Overton, K. W. & Wang, C. L. Tuning gene expression with synthetic upstream open reading frames. *Proc. Natl Acad. Sci. USA* **110**, 11284–11289 (2013).
62. Cerma, T. et al. Efficient design and assembly of custom TALEN and other TAL effector-based constructs for DNA targeting. *Nucleic Acids Res.* **39**, e82 (2011).
63. Doyle, E. L. et al. TAL Effector-Nucleotide Targeter (TALE-NT) 2.0: tools for TAL effector design and target prediction. *Nucleic Acids Res.* **40**, W117–W122 (2012).
64. Sanjana, N. E. et al. A transcription activator-like effector toolbox for genome engineering. *Nat. Protoc.* **7**, 171–192 (2012).
65. Shiau, C. E., Monk, K. R., Joo, W. & Talbot, W. S. An anti-inflammatory NOD-like receptor is required for microglia development. *Cell Rep.* **5**, 1342–1352 (2013).

nature research

Corresponding author(s): DBPR NCB-M35531A

Last updated by author(s): 1/14/2019

Reporting Summary

Nature Research wishes to improve the reproducibility of the work that we publish. This form provides structure for consistency and transparency in reporting. For further information on Nature Research policies, see Authors & Referees and the Editorial Policy Checklist.

Statistics

For all statistical analyses, confirm that the following items are present in the figure legend, table legend, main text, or Methods section.

n/a	Confirmed	
☐	☒	The exact sample size (*n*) for each experimental group/condition, given as a discrete number and unit of measurement
☐	☒	A statement on whether measurements were taken from distinct samples or whether the same sample was measured repeatedly
☐	☒	The statistical test(s) used AND whether they are one- or two-sided *Only common tests should be described solely by name; describe more complex techniques in the Methods section.*
☒	☐	A description of all covariates tested
☒	☐	A description of any assumptions or corrections, such as tests of normality and adjustment for multiple comparisons
☐	☒	A full description of the statistical parameters including central tendency (e.g. means) or other basic estimates (e.g. regression coefficient) AND variation (e.g. standard deviation) or associated estimates of uncertainty (e.g. confidence intervals)
☐	☒	For null hypothesis testing, the test statistic (e.g. *F*, *t*, *r*) with confidence intervals, effect sizes, degrees of freedom and *P* value noted *Give P values as exact values whenever suitable.*
☒	☐	For Bayesian analysis, information on the choice of priors and Markov chain Monte Carlo settings
☒	☐	For hierarchical and complex designs, identification of the appropriate level for tests and full reporting of outcomes
☒	☐	Estimates of effect sizes (e.g. Cohen's *d*, Pearson's *r*), indicating how they were calculated

Our web collection on statistics for biologists contains articles on many of the points above.

Software and code

Policy information about availability of computer code

Data collection	Slidebook6 (FRAP, Plasma membrane translocation and Lysotracker Green experiments) ; Metamorph/MetaXpress (experiments measuring lysosome localization, phospho-rpS6, phospho-4E-BP1, p62, and LC3-GFP)
Data analysis	lysosome localization: custom Matlab (2009) script. p62, Lystracker Green and LC3-GFP: custom Matlab script. phospho-rpS6 and phospho-4E-BP1: CellProfiler 1.0.0. FRAP: ImageJ 1.50b and curve fitting by GraphPadPrism 5.

For manuscripts utilizing custom algorithms or software that are central to the research but not yet described in published literature, software must be made available to editors/reviewers. We strongly encourage code deposition in a community repository (e.g. GitHub). See the Nature Research guidelines for submitting code & software for further information.

Data

Policy information about availability of data

All manuscripts must include a data availability statement. This statement should provide the following information, where applicable:

- Accession codes, unique identifiers, or web links for publicly available datasets
- A list of figures that have associated raw data
- A description of any restrictions on data availability

Statistical source data for Figs. 2–8 and Supplementary Figs. 1, 2, 4-6 and 8 are provided in Supplementary Table 4 and unprocessed images of all gels in Figures 2, 4 and 5 will be provided as an additional Supplementary Figure.

Field-specific reporting

Please select the one below that is the best fit for your research. If you are not sure, read the appropriate sections before making your selection.

☒ Life sciences ☐ Behavioural & social sciences ☐ Ecological, evolutionary & environmental sciences

For a reference copy of the document with all sections, see nature.com/documents/nr-reporting-summary-flat.pdf

Life sciences study design

All studies must disclose on these points even when the disclosure is negative.

Sample size	For screen optimization for the primary phospho-rpS6 screen and secondary mTOR translocation screen, we observed that triplicate wells in 384 well format and duplicate wells in 96 well format showed good reproducibility across experiments for our assay conditions. For immunofluorescence experiments, we always use at least 2 wells in 96 well format for each independent experiment. There are >1000 cells in a single 96 well analyzed and give us sufficient n to make statistically-meaningful comparisons among different treatments. For FRAP and plasma membrane translocation experiments, we use standards commonly adopted in the field to make statistically-meaningful comparisons.
Data exclusions	No data was excluded from the results reported here.
Replication	Experiments reported here were performed at least twice. All attempts at replication were successful. For FRAP experiment repeats included in Figure 6k, we sometimes increased the n to >30 lysosomes for each condition to make sure the phenotype we are seeing is representative of the population because lysosomes move fast or split off which can result in noisy single recovery curves.
Randomization	*Describe how samples/organisms/participants were allocated into experimental groups. If allocation was not random, describe how covariates were controlled OR if this is not relevant to your study, explain why.*
Blinding	For lysosome localization studies, lysosomes were first masked in the Lamp2 channel and mTOR or other proteins were then measured. Similarly for FRAP studies, lysosomes were first tracked using a lysosome marker (i.e Lamp1-Turquoise) and then RagC intensity in the mask was measured.

Reporting for specific materials, systems and methods

We require information from authors about some types of materials, experimental systems and methods used in many studies. Here, indicate whether each material, system or method listed is relevant to your study. If you are not sure if a list item applies to your research, read the appropriate section before selecting a response.

Materials & experimental systems

n/a	Involved in the study
☐	☒ Antibodies
☐	☒ Eukaryotic cell lines
☐	☐ Palaeontology
☐	☒ Animals and other organisms
☐	☐ Human research participants
☐	☐ Clinical data

Methods

n/a	Involved in the study
☐	☐ ChIP-seq
☐	☐ Flow cytometry
☐	☐ MRI-based neuroimaging

Antibodies

Antibodies used	Please see Antibodies information in Supplementary Table 5
Validation	Antibodies were validated by the manufacturer and we validated the antibodies using RNAi and also checking their localization was consistent with literature reports.

Eukaryotic cell lines

Policy information about cell lines

Cell line source(s)	HS68, HeLa and HEK293T cells were purchased from ATCC; Parental and CRISPR-Cas9 edited HAP-1 cells were purchased from Horizon Discovery; RagA/B null and parental MEFs were provided by Dr. Kun-Liang Guan's lab, and sgNprl3 and parental HEK293E cells, sgSestrin 1/2/3 and parental HEK293T cells were provided by Dr. David Sabatini's lab.
Authentication	HS68, HeLa and HEK293Ts were authenticated by ATCC. RagA/B null MEFs were authenticated by staining for RagA and RagC (RagC/D also are depleted when RagA/B are missing). sgNprl3 and sgSestrin 1/2/3 were not authenticated but showed the

	predicted functional phenotype (i.e constitutively-active mTORC1 tranlsocation or higher basal mTORC1 translocation in starved conditions).
Mycoplasma contamination	HS68, HeLa and HEK293T cells were tested negative for mycoplasma contamination. RagA/B null, sgNprl3, and sgSestrin 1/2/3 and their parental cells were not tested for mycoplasma contamination.
Commonly misidentified lines (See ICLAC register)	No cell lines used in this study were found in the database of commonly misidentified cell lines that is maintained by ICLAC and NCBI Biosample.

Palaeontology

Specimen provenance	*Provide provenance information for specimens and describe permits that were obtained for the work (including the name of the issuing authority, the date of issue, and any identifying information).*
Specimen deposition	*Indicate where the specimens have been deposited to permit free access by other researchers.*
Dating methods	*If new dates are provided, describe how they were obtained (e.g. collection, storage, sample pretreatment and measurement), where they were obtained (i.e. lab name), the calibration program and the protocol for quality assurance OR state that no new dates are provided.*

☐ Tick this box to confirm that the raw and calibrated dates are available in the paper or in Supplementary Information.

Animals and other organisms

Policy information about studies involving animals; ARRIVE guidelines recommended for reporting animal research

Laboratory animals	Wildtype, gpr137ba+/-, gpr137ba-/- zebrafish, both males and females between 4-5 dpf were used.
Wild animals	The study did not involve wild animals.
Field-collected samples	The study did not involve samples collected from the field.
Ethics oversight	Stanford University Institutional Animal Care and Use Committee approved the zebrafish protocol.

Note that full information on the approval of the study protocol must also be provided in the manuscript.

Human research participants

Policy information about studies involving human research participants

Population characteristics	*Describe the covariate-relevant population characteristics of the human research participants (e.g. age, gender, genotypic information, past and current diagnosis and treatment categories). If you filled out the behavioural & social sciences study design questions and have nothing to add here, write "See above."*
Recruitment	*Describe how participants were recruited. Outline any potential self-selection bias or other biases that may be present and how these are likely to impact results.*
Ethics oversight	*Identify the organization(s) that approved the study protocol.*

Note that full information on the approval of the study protocol must also be provided in the manuscript.

Clinical data

Policy information about clinical studies

All manuscripts should comply with the ICMJE guidelines for publication of clinical research and a completed CONSORT checklist must be included with all submissions.

Clinical trial registration	*Provide the trial registration number from ClinicalTrials.gov or an equivalent agency.*
Study protocol	*Note where the full trial protocol can be accessed OR if not available, explain why.*
Data collection	*Describe the settings and locales of data collection, noting the time periods of recruitment and data collection.*
Outcomes	*Describe how you pre-defined primary and secondary outcome measures and how you assessed these measures.*

ChIP-seq

Data deposition

☐ Confirm that both raw and final processed data have been deposited in a public database such as GEO.

☐ Confirm that you have deposited or provided access to graph files (e.g. BED files) for the called peaks.

Data access links *May remain private before publication.*	*For "Initial submission" or "Revised version" documents, provide reviewer access links. For your "Final submission" document, provide a link to the deposited data.*
Files in database submission	*Provide a list of all files available in the database submission.*
Genome browser session (e.g. UCSC)	*Provide a link to an anonymized genome browser session for "Initial submission" and "Revised version" documents only, to enable peer review. Write "no longer applicable" for "Final submission" documents.*

Methodology

Replicates	*Describe the experimental replicates, specifying number, type and replicate agreement.*
Sequencing depth	*Describe the sequencing depth for each experiment, providing the total number of reads, uniquely mapped reads, length of reads and whether they were paired- or single-end.*
Antibodies	*Describe the antibodies used for the ChIP-seq experiments; as applicable, provide supplier name, catalog number, clone name, and lot number.*
Peak calling parameters	*Specify the command line program and parameters used for read mapping and peak calling, including the ChIP, control and index files used.*
Data quality	*Describe the methods used to ensure data quality in full detail, including how many peaks are at FDR 5% and above 5-fold enrichment.*
Software	*Describe the software used to collect and analyze the ChIP-seq data. For custom code that has been deposited into a community repository, provide accession details.*

Flow Cytometry

Plots

Confirm that:

☐ The axis labels state the marker and fluorochrome used (e.g. CD4-FITC).

☐ The axis scales are clearly visible. Include numbers along axes only for bottom left plot of group (a 'group' is an analysis of identical markers).

☐ All plots are contour plots with outliers or pseudocolor plots.

☐ A numerical value for number of cells or percentage (with statistics) is provided.

Methodology

Sample preparation	*Describe the sample preparation, detailing the biological source of the cells and any tissue processing steps used.*
Instrument	*Identify the instrument used for data collection, specifying make and model number.*
Software	*Describe the software used to collect and analyze the flow cytometry data. For custom code that has been deposited into a community repository, provide accession details.*
Cell population abundance	*Describe the abundance of the relevant cell populations within post-sort fractions, providing details on the purity of the samples and how it was determined.*
Gating strategy	*Describe the gating strategy used for all relevant experiments, specifying the preliminary FSC/SSC gates of the starting cell population, indicating where boundaries between "positive" and "negative" staining cell populations are defined.*

☐ Tick this box to confirm that a figure exemplifying the gating strategy is provided in the Supplementary Information.

Magnetic resonance imaging

Experimental design

Design type	*Indicate task or resting state; event-related or block design.*

Design specifications

Specify the number of blocks, trials or experimental units per session and/or subject, and specify the length of each trial or block (if trials are blocked) and interval between trials.

Behavioral performance measures

State number and/or type of variables recorded (e.g. correct button press, response time) and what statistics were used to establish that the subjects were performing the task as expected (e.g. mean, range, and/or standard deviation across subjects).

Acquisition

Imaging type(s)

Specify: functional, structural, diffusion, perfusion.

Field strength

Specify in Tesla

Sequence & imaging parameters

Specify the pulse sequence type (gradient echo, spin echo, etc.), imaging type (EPI, spiral, etc.), field of view, matrix size, slice thickness, orientation and TE/TR/flip angle.

Area of acquisition

State whether a whole brain scan was used OR define the area of acquisition, describing how the region was determined.

Diffusion MRI ☐ Used ☐ Not used

Preprocessing

Preprocessing software

Provide detail on software version and revision number and on specific parameters (model/functions, brain extraction, segmentation, smoothing kernel size, etc.).

Normalization

If data were normalized/standardized, describe the approach(es): specify linear or non-linear and define image types used for transformation OR indicate that data were not normalized and explain rationale for lack of normalization.

Normalization template

Describe the template used for normalization/transformation, specifying subject space or group standardized space (e.g. original Talairach, MNI305, ICBM152) OR indicate that the data were not normalized.

Noise and artifact removal

Describe your procedure(s) for artifact and structured noise removal, specifying motion parameters, tissue signals and physiological signals (heart rate, respiration).

Volume censoring

Define your software and/or method and criteria for volume censoring, and state the extent of such censoring.

Statistical modeling & inference

Model type and settings

Specify type (mass univariate, multivariate, RSA, predictive, etc.) and describe essential details of the model at the first and second levels (e.g. fixed, random or mixed effects; drift or auto-correlation).

Effect(s) tested

Define precise effect in terms of the task or stimulus conditions instead of psychological concepts and indicate whether ANOVA or factorial designs were used.

Specify type of analysis: ☐ Whole brain ☐ ROI-based ☐ Both

Statistic type for inference
(See Eklund et al. 2016)

Specify voxel-wise or cluster-wise and report all relevant parameters for cluster-wise methods.

Correction

Describe the type of correction and how it is obtained for multiple comparisons (e.g. FWE, FDR, permutation or Monte Carlo).

Models & analysis

n/a	Involved in the study
☐	☐ Functional and/or effective connectivity
☐	☐ Graph analysis
☐	☐ Multivariate modeling or predictive analysis

Functional and/or effective connectivity

Report the measures of dependence used and the model details (e.g. Pearson correlation, partial correlation, mutual information).

Graph analysis

Report the dependent variable and connectivity measure, specifying weighted graph or binarized graph, subject- or group-level, and the global and/or node summaries used (e.g. clustering coefficient, efficiency, etc.).

Multivariate modeling and predictive analysis

Specify independent variables, features extraction and dimension reduction, model, training and evaluation metrics.